Available online at www.sciencedirect.com
SCIENCE DIRECT
Geochimica et Cosmochimica Acta 70 (2006) 3717–3742
Geochimica
www.elsevier.com/locate/gca

# Trace element partitioning in plagioclase feldspar

Jean H. Bédard *

*Geological Survey of Canada, 490 de la Couronne, Quebec, PQ, Canada G1K 9A9*

Received 12 July 2005; accepted in revised form 3 May 2006

**Abstract**

Compilation and interpretation of experimental and natural Nernst partition coefficient ($^{plagioclase/melt}D$) data show that, with a few exceptions, increases in $^{plagioclase/melt}D$ correlate with decreasing anorthite-content of plagioclase. In contrast, increases of $^{plagioclase/melt}D$ for Ga, Sc, Cu, Zn, Zr, Hf and Ti, are better correlated against decreasing melt MgO or increasing melt $SiO_2$ contents. $^{plagioclase/melt}D$ for Ti and the rare earth elements (REE) show little dependence on temperature, but increase as the melt water content increases. $^{plagioclase/melt}D$ for K and Sr are sensitive to pressure. Variations of $D_0$ (the strain compensated partition coefficient), $r_0$ (the size of the site into which REE substitute), and $E$ (Young's Modulus of this site) were parameterized against variations of melt $SiO_2$, the An-content of plagioclase, and other combinations of variables, allowing $^{plagioclase/melt}D_{REE\text{-}Y}$ to be calculated from a variety of input parameters. The interrelations of temperature, melt MgO and $SiO_2$ content, and plagioclase anorthite-content for wet and dry systems were also parameterized to facilitate interpolation where such data are lacking. When combined, these semi-empirical parameterizations yield $^{plagioclase/melt}D$ results comparable to available experimental and natural data.


## 1. Introduction

### 1.1. Plagioclase and D

The Nernst partition coefficient '$D$' is the ratio of the weight concentration of a trace element in a solid phase divided by the concentration of the same element in its equilibrium liquid ($D = C_s/C_l$), and is used extensively to model magmatic processes (e.g. Treuil and Varet, 1973; Langmuir, 1989; O'Hara, 1995; Shaw, 2000). The uncertainty with regard to $D$ is a major source of error in modeling crystal/liquid fractionation or melting, and in applying inversion models to cumulates or restites (Blundy, 1997; Bédard, 1994, 2001). Plagioclase feldspar is the dominant mineral in the terrestrial continental crust and lunar highlands crust, is abundant in the lower oceanic crust, and also occurs in oceanic upper mantle rocks and some meteorites (e.g. Gass et al., 1984; Beckett and Grossman, 1988; Smith and Brown, 1988). In low-pressure terrestrial lavas, plagioclase occurs throughout the magmatic compositional spectrum from basalt to rhyolite (e.g. Grove et al., 1982; Spulber and Rutherford, 1983; Villiger et al., 2004). Plagioclase fractionates trace elements of similar size and valency (e.g. $^{plagioclase/melt}D_{La}/^{plagioclase/melt}D_{Yb}$ is between 5 and 35), leading to relative light rare earth element depletion in derivative liquids. Plagioclase also concentrates Sr and Eu, generating the diagnostic positive trace element peaks indicative of plagioclase accumulation in gabbroic rocks, and negative peaks indicative of plagioclase extraction in derivative liquids.

Until the groundbreaking paper of Blundy and Wood (1991), who parameterized $^{plagioclase/melt}D$ variations of Sr and Ba against temperature and the anorthite-content of plagioclase (An = Ca/Ca + Na + K), most trace element modeling studies assumed that values of $^{plagioclase/melt}D$ were constants. Bindeman et al. (1998) and Bindeman and Davis (2000) extended this approach to a wider range of trace elements, and pointed out problems with experiments involving doping. Available experimental and natural partitioning studies were compiled in an effort to complete and update these previous studies.

* Fax: +1 418 654 2615.
*E-mail address:* jbedard@rncan.gc.ca.

0016-7037/$ - see front matter 
doi:10.1016/j.gca.2006.05.003

Table 1
Data sources used in this paper

*Experimental data*
B = Baker and Eggler (1987)
b = Bartels et al. (1991)
b1 = Berndt (2002)
b2 = Bindeman et al. (1998)
b3 = Bindeman and Davis (2000)
b4 = Blatter and Carmichael (2001)
b5 = Blundy (1997)
b6 = Blundy et al. (1998)
b7 = Brugger et al. (2003)
b8 = Beard et al. (1993)
b9 = Berndt et al. (2001)
C = Carroll and Wyllie (1989)
c = Costa et al. (2004)
c2 = Couch et al. (2003)
c3 = Capobianco et al. (1991)
D = Drake and Weill (1975)
d1 = Dunn and Sen (1994)
d2 = Duncan and Green (1987)
d3 = Douce and Beard (1995)
d4 = Douce and Beard (1996)
d5 = Douce (2005)
F = Falloon et al. (1999)
f = Fram and Longhi (1992)
f1 = Freise et al. (2003)
G = Grove and Juster (1989)
g = Grove et al. (1982)
g1 = Grove et al. (2003)
g2 = García-Casco et al. (2003)
g3 = Gerke et al. (2005)
H = Holtz et al. (2005)
j = Johnston (1986)
K = Kinzler and Grove (1992)
k = Koepke et al. (2003)
L = Longhi et al. (1999)
l2 = López and Castro (2001)
l3 = López et al. (2005)
l4 = Larsen (2005)
M = Montel and Vielzeuf (1997)
m = Moore and Carmichael (1998)
m1 = Müntener et al. (2001)
m2 = Médard et al. (2004)
m3 = Malvin and Drake (1987)
m4 = McKay and Weill (1976)
m5 = McKay and Weill (1977)
m6 = Martel et al. (1999)
m7 = Métrich and Rutherford (1998)
N = Nair and Chacko (2002)
n = Nekvasil et al. (2004)
P = Douce and Harris (1998)
p = Pertermann et al. (2004)
p2 = Prouteau and Scaillet (2003)
p3 = Panjasawatwong et al. (1995)
R = Righter et al. (1995)
S = Scaillet and Evans (1999)
s = Skjerlie and Johnston (1996)
s1 = Schmidt and Thompson (1996)
s2 = Simon et al. (1994)
s3 = Singh and Johannes (1996)
s4 = Springer and Seck (1997)
s5 = Sisson et al. (2005)
T = Thy (1995)
t = Toplis and Carroll (1995) & Toplis et al. (1994)
t1 = Tormey et al. (1987)
t2 = Tuff et al. (2005)
t3 = Takagi et al. (2005)
v = Van der Auwera et al. (2000)
v2 = Villiger et al. (2004)
w = Wilke and Behrens (1999)
y = Yang et al. (1996)

*Natural data*
1 = Arth and Barker (1976)
2 = Bédard (1994)
3 = Bacon and Druitt (1988)
4 = Dodge et al. (1982)
5 = Dostal and Capedri (1975)
6 = Dostal et al. (1983)
7 = Ewart and Griffin (1994)
8 = Francalanci (1989)
9 = Fujimaki et al. (1984)
10 = Gromet and Silver (1983)
11 = Luhr and Carmichael (1980)
12 = Michael (1983)
13 = Nagasawa and Schnetzler (1971)
14 = Nash and Crecraft (1985)
15 = Schnetzler and Philpotts (1968)
16 = Vernières et al. (1977)
17 = Villemant et al. (1980)
18 = Wörner et al. (1983)
19 = Ren et al. (2003)
20 = Dudas et al. (1971)
21 = Phinney and Morrison (1990)

The letter and number codes are those used in all figures.

$^{\text{plagioclase/melt}}D$ data originating from analysis of phenocrysts in lavas or intrusions are referred to as 'natural' data here, and have number codes, while experimental partitioning data are given letter codes. Table 1 gives data sources and codes, which also appear in some figures. For simplicity, sub/superscripts will be left out henceforth (e.g. $D\ \mathrm{Sc} = {}^{\text{plagioclase/melt}}D_{\mathrm{Sc}}$). The dataset is available as an electronic appendix from the author. Mineral/mineral partitioning studies were not considered because of subsolidus reequilibration effects (e.g. McDonough et al., 1992; Loucks, 1996). Much of the data on partitioning of Ti and K were gleaned from phase equilibrium studies. It is the purpose of this paper to synthesize these data in order to provide an objective algebraic parameterization of the values of $D$, and of the dominant trend of variation of $D$ values, which can be used to model igneous processes in common magmatic suites.

### 1.2. Input parameters

What should be the input variable(s) for the parameterization of $D$ variations? The ability to reproduce the data is the main criterion, but ease of application must also be considered. Blundy and Wood (1991) and Bindeman et al. (1998) proposed simple equations of the form:

$$RT \ln D = X\ \mathrm{An} + Y, \tag{A}$$

where $R$ is the gas constant, An is the fraction of anorthite component in plagioclase, $T$ is temperature (Kelvin), while

Table 2
Regression results for interrelation of plagioclase An-content, melt composition and temperature, for wet and dry systems

$T$ in K, $P$ in kbar, Ca# = 100Ca/(Ca + Na); Al# = 100Al/(Al + Si) — Eq. # 1[a]
An mole% = $(-63{,}970/T) - 164.1 - (2575.3\ P/T) + (41.836 \ln(\text{Ca\#melt})) + (33.434 \ln(\text{Al\#melt}))$
$T$ in K, $P$ in bar, An in mole%, $H_2O$ in wt% — Eq. # 2[b]
$\ln An = (927.91/T) - 0.86298 - (0.02693\ P/T) + (0.01674\ H_2O)$

| Unknown | AR-IV | $Y$ intercept | Standard error $Y$ | $R^2$ | $N$ | Slope $X$ | Standard error $X$ | Eq.# |
|---|---|---|---|---|---|---|---|---|
| *An of plagioclase from MgO in melt (wt%), for dry melts (An = X MgO + Y)* | | | | | | | | |
| An molar | MgO > 1% | 0.42132 | 0.07065 | 0.700 | 342 | 0.04448 | 0.00158 | 3a |
| An molar | MgO < 1% | 0.10090 | 0.10362 | 0.572 | 25 | 0.50206 | 0.09061 | 3b |
| | (Intersection of Eqs. 3a and 3b at 0.7003% MgO) | | | | | | | |
| *An of plagioclase from lnMgO in melt (wt%), for wet melts. (An = X lnMgO + Y)* | | | | | | | | |
| An molar | All | 0.57229 | 0.13285 | 0.485 | 610 | 0.10639 | 0.00444 | 3c |
| *Multiple regression: an of plagioclase from T (°C), P (GPa), $H_2O$ (wt%) & Melt lnMgO (wt%)* | | | | | | | | |
| An molar | All | 0.06619 | 0.06042 | 0.5439 | 988 | (SE = 0.112821) | | 4 |
| | $T$ | | | | | 0.00047 | 0.00006 | |
| | $P$ | | | | | −0.10239 | 0.00901 | |
| | $H_2O$ | | | | | 0.02206 | 0.00187 | |
| | lnMgO | | | | | 0.06484 | 0.00530 | |
| *10,000/T (°C) from lnMgO (wt%) of melt, (10,000/T (°C) = X lnMgO + Y)* | | | | | | | | |
| lnMgO | All | 10.3758 | 0.0232 | 0.7513 | 1015 | −0.95668 | 0.01728 | 5a |
| $T$ (°C) from $SiO_2$ wt% of melt, ($T$ (°C) = $X$ $SiO_2$ + $Y$) | | | | | | | | |
| $SiO_2$ | All | 1712.0 | 90.26 | 0.6206 | 577 | −11.691 | 0.3618 | 5b |

Unknown, value to be calculated. AR-IV, applicable range (AR) for regression, and/or, (IV) input variable from which the unknown is calculated. Estimates of the errors on the regressions and the fit ($R^2$) are also given. In the multiple regressions, SE: standard error.

[a] From Panjasawatwong et al. (1995).

[b] From Takagi et al. (2005).

'*X*' is the slope and '*Y*' the intercept in an $RT\ln D$ vs. An plot. Use of the '*RT*' factor partly corrects for the influence of temperature and slightly improves the fits (Blundy and Wood, 1991). Pressure and temperature (Shimizu, 1974; Green and Pearson, 1985), melt composition (Mysen and Virgo, 1980; Nielsen, 1985; Gaetani, 2004), and melt $H_2O$ content (Wood and Blundy, 2002), have been advocated as important factors responsible for *D*-variations in other minerals, but these effects have not been explored as systematically for plagioclase. Indices of melt compositional evolution considered here are the $SiO_2$ and MgO contents, the values of which can be calculated from coexisting minerals through the application of exchange and distribution coefficients (e.g. Markl and Frost, 1999; Sugawara, 2000); or which can be constrained empirically from lava, glass or melt inclusion analyses.

A multiple linear regression approach was used to constrain *D* variations where the database was adequate. However, a complete range of possible input parameters is not found in each experiment or natural partitioning dataset. Some are simplified systems, while others do not provide complete melt or mineral analyses. Furthermore, natural partitioning observations cannot provide exact values for pressure or temperature. Consequently, datasets that lack certain input variables cannot be included in many multiple regression analyses. In addition, many modeling situations, such as inversions applied to cumulate rocks, do not provide the necessary input (e.g. knowledge of the melt composition, temperature, pressure, volatile contents) for such an approach. Since the 'bottom-line' is useability, a simplified approach that considers fewer input parameters is also included. While inherently less precise than a simultaneous consideration of the influence of all potential input variables on *D* variations, the simplified approach at least has the benefit of being applicable to all modeling scenarios, including inverse calculations. Where possible, both the simple regressions and the multiple regression analyses are provided, to give modelers flexibility.

This partly empirical approach is not meant as a substitute for thermodynamically based partitioning models (e.g. Beattie et al., 1991; Blundy et al., 1996; Wood and Blundy, 1997; Gaetani, 2004). However, despite the con-

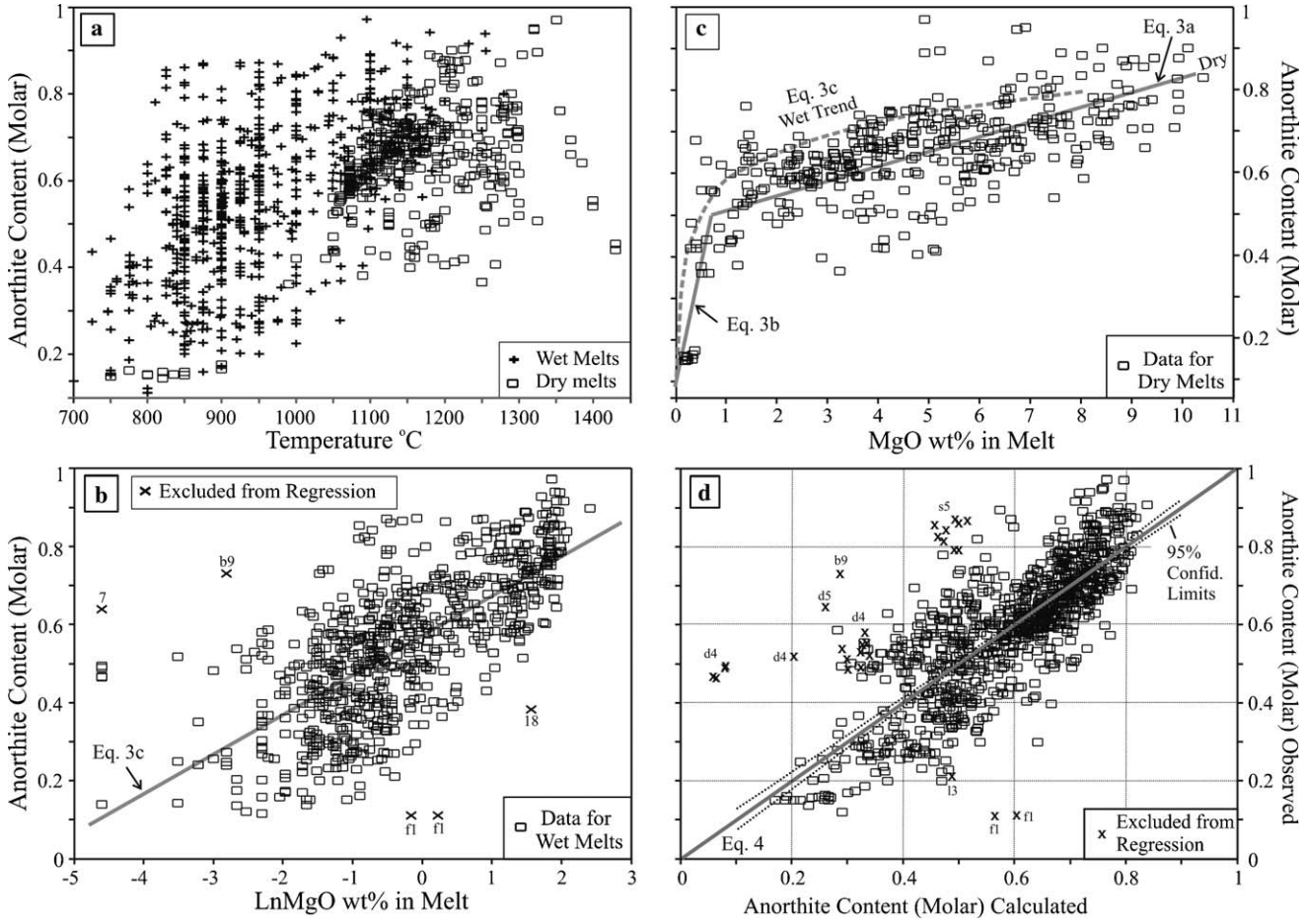


Fig. 1. Plagioclase An-content plotted against: (a) temperature in °C, (b) melt lnMgO (wt%) content for wet systems, and (c) for dry systems. Note the extensive scatter in the 'wet' data (a), and the generally higher An-contents of the 'wet'data for a given temperature. (b) Regression for data from 'wet' systems plotted against lnMgO (Eq. 3c, Table 2). (c) Regression for data from 'dry' systems plotted against melt MgO (Eqs. 3a,b. Table 2), with the regression from (b, wet systems) shown as a dashed line. (d) Comparison of observed An-contents with those calculated with Eq. 4, Table 2.

siderable progress achieved in their development (e.g. Blundy and Wood, 2003), it is not yet possible to obtain the values of $D$ for all trace elements and $P$–$T$–$X$ conditions of interest from such theoretical models, or to quantify how the $D$s vary; and realistically, it will be many years before this becomes possible. For those needing a set of $D$ values to model a given magmatic suite, a common sense approach has been to use $D$ values from an experiment conducted at appropriate pressure–temperature conditions on a melt composition that is 'similar' to the suite being investigated. However: (a) few bulk compositions have been investigated in enough detail to do this; (b) few partitioning studies consider the entire geochemical spectrum, handicapping users of multi-element plots (e.g. Thompson et al., 1983); and (c) the extent to which $D$s vary with changing $P$–$T$–$X$ conditions would still not be accounted for. Given the need for a systematic, quantitative, multi-element estimate of $^{\text{plagioclase/melt}}D$, and for how these $D$s vary, the semi-empirical parameterizations proposed here represent an interim, practical solution, which at least provides a realistic estimate of the uncertainty in $D$, and which may help guide subsequent experimental efforts.

### 1.3. Sources of error and uncertainty

This is a compilation of data from both experimental and natural partitioning studies, analyzed over a span of 25 years with different methods in different laboratories. Consequently, one has to consider the probability of inter-laboratory biases, the progressive improvements in precision and accuracy that have occurred, the possibility that kinetic or pneumatolytic effects perturbed some experiments or observations, and finally, the probability of experimental or typographical errors. When analyzing the partitioning data, discrepant datapoints were excluded from some regressions. Although discrepant data that result from experimental errors can safely be neglected, data outliers could also reflect systematic differences in pressure, $f_{O_2}$, volatile activity, bulk composition, crystal chemistry…, etc. These alternatives were investigated where the database was adequate, but it was not always possible to determine why some datapoints or datasets were discrepant. There are four main groups of discrepant data: (1) those from older datasets, (2) natural data (phenocryst/matrix or phenocryst/whole-rock), (3) data obtained from phase equilibrium studies, and (4) data from synthetic bulk compositions.

(1) The anomalous values of some older data presumably represent analytical limitations, and after comparison, some of the most discrepant older data were excluded from the regressions. (2) Partitioning data obtained from natural phenocryst/matrix pairs are not as well constrained as experimental data because: (a) $D$ is commonly calculated assuming that the matrix or bulk composition represents liquid compositions, (b) the assemblage may not be in equilibrium (e.g. Albarède and Bottinga, 1972; Tepley et al., 2000; Perugini et al., 2003), (c) the potential effects of mineral or melt inclusions in mineral separates are not always considered (e.g. Michael, 1988; Lutz, 1991), and (d) temperature and pressure are rarely constrained. Nevertheless, although treated with caution, many of these 'natural' partitioning values are also considered here because there are no experimental data available for some elements and melt compositional ranges. (3) A potential problem with partitioning data obtained from phase equilibrium studies (Ti, K), is that routine minor element analyses may not

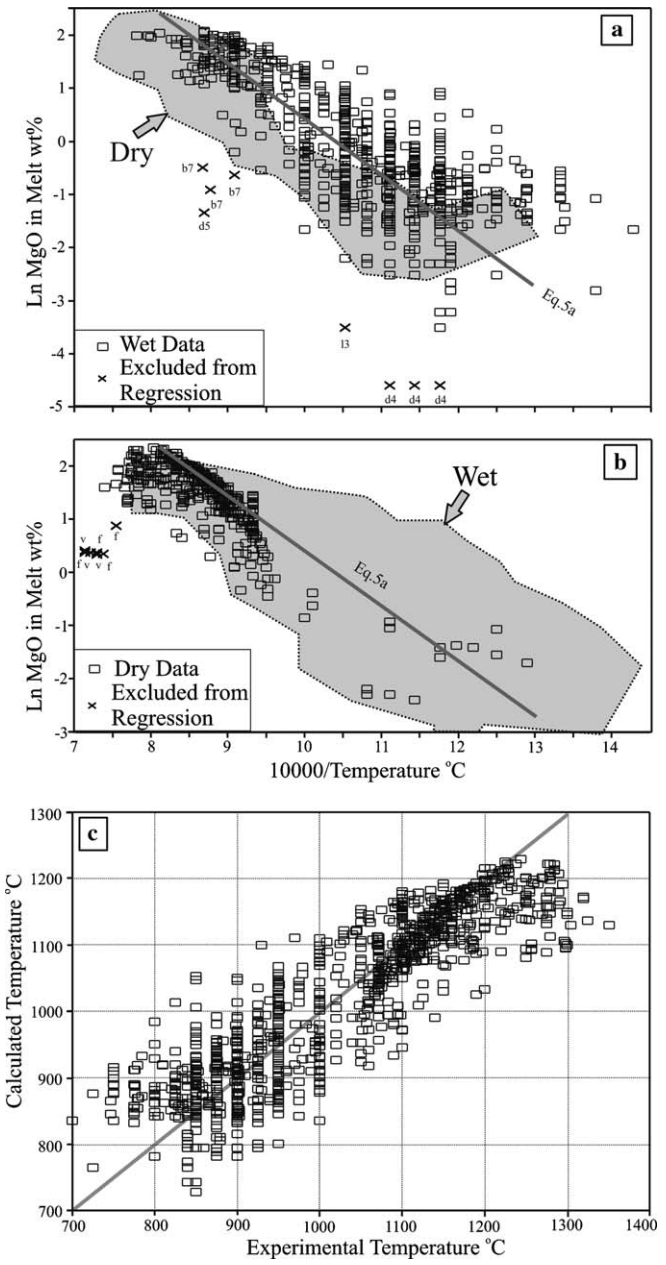


Fig. 2. LnMgO (wt%) in the melt plotted against 10,000/temperature °C, for wet (a) and dry (b) systems (Eq. 5, Table 2). (c) Compares results calculated from the MgO-$T$ °C regressions (Eq. 5) against experimental temperatures.

have been controlled as carefully as in the dedicated partitioning studies. However, while inclusion of natural and phase equilibrium data increases scatter somewhat, it also provides improved coverage of the $P$–$T$–$X$ spectrum. (4) Some experimental studies use synthetic bulk compositions that are very different from natural melts; which affected the value of the partition coefficient, at least in some cases.

### 1.4. Approach

First, I parameterize the distribution of data linking the An-content of plagioclase to temperature, pressure and melt composition (Table 2, Figs. 1 and 2). These equations will be used to model natural data in terms of $RT \ln D$ against variations of An-content or melt composition. Because $TiO_2$ and $K_2O$ can be analyzed with the electron microprobe, the $D$ Ti and $D$ K datasets are large enough to allow causal mechanisms to be explored (Tables 3 and 4, Figs. 3–7), providing insight when considering smaller datasets for geochemically similar elements. Similar regressions were performed for all elements where sufficient data exist (Figs. 7–13, Table 4), and a choice of input parameters is provided wherever possible, which allows flexibility in different modeling scenarios. The best regression coefficients obtained are provided in the Tables. Where no perceptible correlations were found, or data are too scanty, averages were computed (Table 4). Comparisons of the regression results for $D$ REE-Y (Fig. 14) with the Lattice Strain Model of Blundy and Wood (1994) were then used to derive equations linking a variety of input variables with $D_0$ (the strain compensated partition coefficient), $E$ (Young's Modulus), and $r_0$ (the size of the REE-hosting site) (Fig. 15, Table 5). From

Table 3
Regression results for variations of $^{plagioclase/melt}D$ Ti against different input parameters, including anorthite content of plagioclase, temperature, melt composition, pressure and water content

| Unknown | AR-IV | $Y$ intercept | Standard error $Y$ | $R^2$ | $N$ | Slope $X$ | Standard error $X$ | Eq. # |
|---|---|---|---|---|---|---|---|---|
| *D Ti calculated from multiple regression* | | | | | | | | |
| ln $D$ Ti | All | −4.6605 | 0.86819 | 0.4939 | 318 | (SE = 0.60362) | | 6 |
| | $H_2O$ melt (wt%) | | | | | 0.07382 | 0.02449 | |
| | $SiO_2$ melt (wt%) | | | | | 0.02367 | 0.00756 | |
| | lnMgO melt (wt%) | | | | | −0.22775 | 0.09312 | |
| | Molar An | | | | | 0.31542 | 0.37651 | |
| | 10,000 $T$ (°C) | | | | | 0.06912 | 0.06602 | |
| | $P$ (GPa) | | | | | −0.22462 | 0.09078 | |
| *D Ti calculated from An-content of plagioclase, (e.g. RT ln D Ti = X An + Y)* | | | | | | | | |
| ln $D$ Ti | An (all) | −1.7503 | 0.83827 | 0.0356 | 344 | −1.2279 | 0.34538 | 7 |
| $RT$ ln $D$ Ti | An (all) | −18.482 | 10.594 | 0.0394 | 344 | −16.353 | 4.3651 | 8 |
| *Binned data for D Ti calculated from An-content of plagioclase, using data $P \leqslant 0.2$ GPa, $H_2O \leqslant 1\%$, $SiO_2 < 70\%$* | | | | | | | | |
| $RT$ ln $D$ Ti | (<50% $SiO_2$) | −26.979 | 5.3020 | 0.0113 | 16 | −5.6090 | 14.035 | 9a |
| $RT$ ln$D$ Ti | (50–55%$SiO_2$) | −34.258 | 3.9394 | 0.0048 | 14 | 3.1360 | 13.096 | 9b |
| $RT$ ln $D$ Ti | (55–60% $SiO_2$) | −34.688 | 4.6305 | 0.0007 | 35 | 1.3636 | 9.3100 | 9c |
| $RT$ ln $D$ Ti | (60–70% $SiO_2$) | −22.237 | 4.9308 | 0.1494 | 45 | −22.905 | 8.3352 | 9d |
| $RT$ ln $D$ Ti | (<2% MgO) | −37.560 | 4.7478 | 0.0607 | 14 | 13.301 | 15.107 | 10a |
| $RT$ ln $D$ Ti | (2–4% MgO) | −24.131 | 3.4357 | 0.0861 | 52 | −16.847 | 7.7640 | 10b |
| $RT$ ln $D$ Ti | (4–6% MgO) | −27.972 | 4.9555 | 0.0457 | 28 | −11.544 | 10.346 | 10c |
| $RT$ ln $D$ Ti | (>6% MgO) | −29.506 | 8.2232 | 0.0097 | 16 | −13.738 | 37.177 | 10d |
| $RT$ ln $D$ Ti | (>2% MgO) | −21.825 | 4.9273 | 0.1495 | 96 | −21.067 | 5.1822 | 10e |
| *D Ti calculated from temperature T (°C), using data $P \leqslant 0.2$ GPa, $H_2O \leqslant 1\%$* | | | | | | | | |
| ln $D$ Ti | (60–70% $SiO_2$) | −2.328 | 0.4634 | 0.0028 | 15 | −0.00031 | 0.00164 | 11a |
| ln $D$ Ti | (55–60% $SiO_2$) | −5.248 | 0.3721 | 0.2582 | 16 | 0.00213 | 0.00097 | 11b |
| ln $D$ Ti | (50–55% $SiO_2$) | −3.257 | 0.3957 | 0.0204 | 40 | 0.00030 | 0.00034 | 11c |
| ln $D$ Ti | (<50% $SiO_2$) | −1.941 | 0.3750 | 0.0429 | 44 | −0.00119 | 0.00087 | 11d |
| *D Ti calculated from melt composition, using data $P \leqslant 0.2$ GPa, $H_2O \leqslant 1\%$* | | | | | | | | |
| $RT$ ln $D$ Ti | $SiO_2$ | −61.303 | 4.9825 | 0.2627 | 117 | 0.49849 | 0.07788 | 12a |
| ln $D$ Ti | $SiO_2$ | −5.0543 | 0.40476 | 0.2436 | 117 | 0.03850 | 0.00633 | 12b |
| $RT$ ln $D$ Ti | lnMgO | −24.073 | 5.5006 | 0.5533 | 126 | −8.6543 | 0.69838 | 12c |
| ln $D$ Ti | lnMgO | −2.1707 | 0.49347 | 0.4689 | 126 | −0.65548 | 0.06265 | 12d |
| *D Ti calculated from pressure (GPa), $SiO_2 < 70\%$, $H_2O < 5\%$* | | | | | | | | |
| $D$ Ti | (All) | 0.058927 | 0.029734 | 0.0319 | 171 | −0.010135 | 0.004295 | 13 |
| *D Ti calculated from melt $H_2O$ (wt%), $P \leqslant 0.2$ GPa* | | | | | | | | |
| *D Ti* | (All) | 0.05378 | 0.06303 | 0.3846 | 205 | 0.02692 | 0.00239 | 14a |
| $RT$ ln $D$ Ti | (All) | −33.256 | 8.2417 | 0.3044 | 217 | 2.9409 | 0.30318 | 14b |

Values of the slope '$X$,' and intercept '$Y$' allow $D$ values to be calculated. Estimates of the errors on the regressions and the fit ($R^2$) are also given. In the multiple regressions, SE, standard error. AR-IV, see Table 2. Filt, filtered data.

Table 4
Regression results for variations of $^{plagioclase/melt}D$ against different input parameters

| | AR-IV | *Y* intercept | Standard error *Y* | $R^2$ | *N* | Slope *X* | Standard error *X* | Eq. # |
|---|---|---|---|---|---|---|---|---|
| Unknown | | | | | | | | |
| $RT \ln D$ K | An (all) | −9.8186 | 5.9362 | 0.1346 | 653 | −14.810 | 1.4721 | 15a |
| $RT \ln D$ K | An (filt1) | −8.6971 | 5.1627 | 0.2043 | 629 | −16.745 | 1.3199 | 15b |
| $RT \ln D$ K | An (filt2) | −8.2080 | 5.1994 | 0.2170 | 593 | −17.907 | 1.3990 | 15c |
| $RT \ln D$ K | An ($P < 0.6$) | −10.548 | 5.0160 | 0.1331 | 395 | −14.788 | 1.9039 | 15d |
| $RT \ln D$ K | *P* (all) | −19.998 | 6.1880 | 0.0587 | 583 | 3.1842 | 0.52880 | 15e |
| $RT \ln D$ K | *P* (filt) | −20.033 | 5.7937 | 0.0735 | 578 | 3.4265 | 0.50683 | 15f |
| $RT \ln D$ K | *P* (3–7% MgO) | −20.206 | 5.8687 | 0.1367 | 179 | 4.9554 | 0.93611 | 15g |
| $RT \ln D$ K | | 7.3596 | 2.9861 | 0.3042 | 561 | (SE = 5.0347) | | 15h |
| | $SiO_2$ melt (wt%) | | | | | −0.1874 | 0.03778 | |
| | MgO melt (wt%) | | | | | 0.4466 | 0.16583 | |
| | Molar An | | | | | −26.777 | 1.9940 | |
| | *P* (GPa) | | | | | 1.5259 | 0.46828 | |
| $RT \ln D$ Cs | An | −12.801 | 5.8636 | 0.4674 | 27 | −32.184 | 6.8700 | 16 |
| $RT \ln D$ Rb | An | −12.208 | 8.1457 | 0.4674 | 90 | −43.564 | 4.9573 | 17 |
| $RT \ln D$ Ba | An (filt) | 10.146 | 5.5904 | 0.6013 | 107 | −35.204 | 2.7975 | 18a |
| $RT \ln D$ Ba | (filt) | −15.889 | 10.5904 | 0.6060 | 84 | (SE = 5.6223) | | 18b |
| | $SiO_2$ melt (wt%) | | | | | 0.3082 | 0.12517 | |
| | Molar An | | | | | −23.1593 | 5.5402 | |
| $RT \ln D$ Sr | An (Dry Low P) | 23.856 | 3.5815 | 0.5653 | 107 | −20.710 | 1.7723 | 19a |
| $RT \ln D$ Sr | *P* (GPa) | 13.238 | 3.1865 | 0.7090 | 9 | −5.6447 | 1.3668 | 19b |
| *D* Sr | *P* (GPa) | 3.8196 | 1.3171 | 0.4723 | 9 | −1.4140 | 0.5649 | 19c |
| $RT \ln D$ Sr | $H_2O$ | 11.331 | 5.8482 | 0.1997 | 89 | 1.9205 | 0.4121 | 19d |
| *D*Sr | $H_2O$ | 4.1253 | 5.1243 | 0.1560 | 89 | 1.4480 | 0.3611 | 19e |
| $RT \ln D$ Sr | | −10.545 | 6.1986 | 0.7021 | 72 | (SE = 3.0354) | | 19f |
| | $H_2O$ melt (wt%) | | | | | 0.7230 | 0.34500 | |
| | $SiO_2$ melt (wt%) | | | | | 0.3964 | 0.08612 | |
| | lnMgO melt (wt%) | | | | | 0.6316 | 0.58071 | |
| | Molar An | | | | | −4.4900 | 3.0256 | |
| $RT \ln D$ Sr | | −9.76305 | 4.87118 | 0.6958 | 79 | (SE = 3.0680) | | 19g |
| | $SiO_2$ melt (wt%) | | | | | 0.38369 | 0.05740 | |
| | Molar An | | | | | −3.4708 | 2.6915 | |
| $RT \ln D$ Pb | An | 0.14815 | 5.5534 | 0.0982 | 30 | −10.4612 | 5.9924 | 20 |
| $\ln D$ Li | An | 1.1839 | 1.0228 | 0.1903 | 45 | −3.4432 | 1.0832 | 21 |
| $RT \ln D$ Be | An | −22.670 | 5.2602 | 0.2090 | 24 | 22.600 | 9.3683 | 22 |
| $RT \ln D$ Cr | An | −4.6191 | 8.2035 | 0.3867 | 26 | −42.901 | 11.028 | 23 |
| $RT \ln D$ Ni | An | 27.795 | 6.9911 | 0.5892 | 10 | −75.474 | 22.283 | 24 |
| $RT \ln D$ Ga | lnMgO | 0.56898 | 4.6441 | 0.4492 | 22 | −1.5845 | 0.39225 | 25a |
| $RT \ln D$ Ga | | −44.089 | 11.8387 | 0.7014 | 22 | (SE = 3.3370) | | 25b |
| | $SiO_2$ melt (wt%) | | | | | 0.5196 | 0.17625 | |
| | lnMgO melt (wt%) | | | | | −0.7780 | 0.92344 | |
| | Molar An | | | | | 21.728 | 5.236 | |
| *D* Ge | MgO | 0.29825 | 0.03673 | 9.4421 | 4 | 0.01567 | 0.01245 | 26 |
| *D* V | An | 0.08875 | 0.00856 | 0.8207 | 4 | −0.09026 | 0.02983 | 27 |
| $RT \ln D$ Sc | MgO | −23.003 | 9.1170 | 0.5586 | 28 | −7.5485 | 1.31594 | 28 |
| $RT \ln D$ Co | An | −11.438 | 7.9950 | 0.2317 | 22 | −20.659 | 8.4125 | 29 |
| $RT \ln D$ Cu | | 37.318 | 115.41 | 0.7427 | 10 | (SE = 6.1292) | | 30 |
| | $SiO_2$ melt (wt%) | | | | | −0.4680 | 1.5490 | |
| | MgO melt (wt%) | | | | | −10.496 | 10.888 | |
| | Molar An | | | | | −11.816 | 14.419 | |
| $RT \ln D$ Zn | MgO | −5.1217 | 8.4797 | 0.3430 | 35 | −6.6545 | 1.6033 | 31 |
| $RT \ln D$ Nb | An | −4.8347 | 17.686 | 0.2345 | 32 | −47.519 | 15.673 | 32a |
| $RT \ln D$ Nb | | −417.35 | 87.943 | 0.7177 | 25 | (SE = 9.7630) | | 32b |
| | $SiO_2$ melt (wt%) | | | | | 5.259 | 1.1641 | |
| | MgO melt (wt%) | | | | | 10.344 | 4.287 | |
| | Molar An | | | | | 40.879 | 14.094 | |
| $RT \ln D$ Ta | | −271.60 | 60.586 | 0.4630 | 18 | (SE = 6.1292) | | 33 |
| | $SiO_2$ melt (wt%) | | | | | 3.157 | 0.8092 | |
| | MgO melt (wt%) | | | | | 8.926 | 3.1641 | |
| | Molar An | | | | | 26.501 | 16.851 | |

(*continued on next page*)

Table 4 (*continued*)

| | AR-IV | *Y* intercept | Standard error *Y* | $R^2$ | *N* | Slope *X* | Standard error *X* | Eq. # |
|---|---|---|---|---|---|---|---|---|
| *RT* ln*D* Zr | (all) An | −0.32496 | 18.0034 | 0.4841 | 74 | −84.6797 | 10.3023 | 34a |
| *RT* ln*D* Zr | (filt) An | 3.6141 | 13.7207 | 0.7102 | 60 | −103.900 | 8.71293 | 34b |
| *RT* ln*D* Zr | (filt) $SiO_2$ | −187.27 | 11.785 | 0.7664 | 62 | 2.26018 | 0.16087 | 35 |
| *RT* ln *D* Zr | (filt) | −191.68 | 12.238 | 0.8004 | 54 | (SE = 10.883) | | 36b |
| | $H_2O$ melt (wt%) | | | | | 1.209 | 0.9973 | |
| | $SiO_2$ melt (wt%) | | | | | 2.290 | 0.1881 | |
| *RT* ln *D* Th | An | −11.646 | 8.9249 | 0.3063 | 36 | −31.369 | 8.0968 | 37 |
| *RT* ln *D* U | An | −7.6146 | 4.6913 | 0.8268 | 17 | −47.279 | 5.5879 | 38a |
| ln *D* U | An | −1.7129 | 0.57865 | 0.4681 | 25 | −2.7716 | 0.61608 | 38b |
| *RT* ln *D* P | An | −17.470 | 3.2816 | 0.3161 | 25 | −19.200 | 5.8891 | 39 |
| *RT* ln *D* Hf | An | −8.2507 | 9.9891 | 0.4577 | 36 | −54.245 | 10.964 | 40a |
| *RT* ln *D* Hf | $SiO_2$ | −126.86 | 6.6721 | 0.7638 | 25 | 1.3989 | 0.16222 | 40b |
| *RT* ln *D* Hf | (filtered) | −146.68 | 41.438 | 0.7496 | 24 | (SE = 6.7687) | | 40c |
| | $SiO_2$ melt (wt%) | | | | | 1.670 | 0.5660 | |
| | MgO melt (wt%) | | | | | 1.276 | 2.4398 | |
| *RT* ln *D* La | An | 2.1146 | 4.8953 | 0.6632 | 63 | −37.009 | 3.3770 | 41a |
| *RT* ln *D* Ce | An | −3.6812 | 4.8375 | 0.6570 | 70 | −33.822 | 2.9636 | 42a |
| *RT* ln *D* Pr | An | −6.8025 | 2.0051 | 0.6849 | 13 | −26.094 | 5.3368 | 43a |
| *RT* ln *D* Nd | An | −5.6996 | 6.5437 | 0.4115 | 69 | −30.850 | 4.5074 | 44a |
| *RT* ln *D* Sm | An | −8.6767 | 7.3051 | 0.4702 | 73 | −33.320 | 4.1974 | 45a |
| *RT* ln *D* Gd | An | −1.9714 | 7.8367 | 0.6629 | 12 | −59.897 | 13.506 | 47a |
| *RT* ln *D* Tb | An | −4.3691 | 4.6964 | 0.7661 | 33 | −44.528 | 4.4196 | 48a |
| *RT* ln *D* Dy | An | −2.2521 | 5.4139 | 0.7774 | 29 | −58.215 | 5.9946 | 49a |
| *RT* ln *D* Y | An | −4.5269 | 7.4062 | 0.6865 | 50 | −51.811 | 5.0540 | 50a |
| *RT* ln *D* Er | An | −8.5000 | 6.3497 | 0.7256 | 14 | −57.253 | 10.164 | 51a |
| *RT* ln *D* Yb | An | −9.2954 | 9.2898 | 0.6056 | 45 | −52.923 | 6.5126 | 52a |
| *RT* ln *D* Lu | An | 0.61501 | 7.2699 | 0.6381 | 23 | −70.378 | 11.565 | 53a |
| *RT* ln *D* La | $SiO_2$ | −70.741 | 5.0674 | 0.7071 | 44 | 0.82717 | 0.08215 | 41b |
| *RT* ln D Ce | $SiO_2$ | −72.837 | 4.9855 | 0.6808 | 50 | 0.79844 | 0.07892 | 42b |
| *RT* ln *D* Nd | $SiO_2$ | −84.698 | 5.1606 | 0.6961 | 47 | 0.96052 | 0.09460 | 44b |
| *RT* ln *D* Sm | $SiO_2$ | −93.113 | 5.6815 | 0.7211 | 52 | 1.02567 | 0.09021 | 45b |
| *RT* ln *D* Eu | $SiO_2$ | −47.071 | 9.8852 | 0.2536 | 55 | 0.68936 | 0.16246 | 46b |
| *RT* ln *D* Gd | $SiO_2$ | −102.76 | 4.1352 | 0.8859 | 8 | 1.16211 | 0.17023 | 47b |
| *RT* ln *D* Tb | $SiO_2$ | −88.152 | 5.2885 | 0.6754 | 24 | 0.93216 | 0.13779 | 48b |
| *RT* ln *D* Dy | $SiO_2$ | −114.16 | 4.9589 | 0.7976 | 28 | 1.26733 | 0.12519 | 49b |
| *RT* ln *D* Y | $SiO_2$ | −121.93 | 8.3243 | 0.6598 | 48 | 1.36846 | 0.14488 | 50b |
| *RT* ln *D* Er | $SiO_2$ | −111.45 | 7.5022 | 0.6399 | 15 | 1.14518 | 0.23826 | 51b |
| *RT* ln *D* Yb | $SiO_2$ | −114.25 | 10.400 | 0.5469 | 39 | 1.17906 | 0.17642 | 52b |
| *RT* ln *D* Lu | $SiO_2$ | −115.04 | 4.6417 | 0.8811 | 17 | 1.26414 | 0.11989 | 53b |
| *RT* ln *D* La | | −43.254 | 13.323 | 0.7262 | 44 | (SE = 4.8426) | | 41c |
| | $SiO_2$ melt (wt%) | | | | | 0.5325 | 0.15351 | |
| | Molar An | | | | | −16.594 | 7.4287 | |
| *RT* ln *D* Ce | | −40.236 | 11.018 | 0.7288 | 50 | (SE = 4.5478) | | 42c |
| | $SiO_2$ melt (wt%) | | | | | 0.4444 | 0.13212 | |
| | Molar An | | | | | −18.566 | 5.7641 | |
| *RT* ln *D* Nd | | −60.108 | 11.019 | 0.7162 | 47 | (SE = 4.9323) | | 44c |
| | $SiO_2$ melt (wt%) | | | | | 0.7080 | 0.14244 | |
| | Molar An | | | | | −16.425 | 7.1601 | |
| *RT* ln *D* Nd | | 9.3313 | 29.755 | 0.8597 | 20 | (SE = 2.9510) | | 44d |
| | $H_2O$ melt (wt%) | | | | | 2.2675 | 1.0709 | |
| | $SiO_2$ melt (wt%) | | | | | −0.27180 | 0.38863 | |
| | MgO melt (wt%) | | | | | −3.8159 | 1.6138 | |
| | Molar An | | | | | − 6.7770 | 11.193 | |
| *RT* ln *D* Sm | | −82.358 | 11.912 | 0.7159 | 52 | (SE = 5.6779) | | 45c |
| | $SiO_2$ melt (wt%) | | | | | 0.9107 | 0.14342 | |
| | Molar An | | | | | −6.1352 | 5.9499 | |
| *RT* ln*D* Eu | | 88.743 | 21.970 | 0.9227 | 17 | (SE = 2.0544) | | 46c |
| | $\log f_{O_2}$ | | | | | −3.0048 | 0.2403 | |
| | $SiO_2$ melt (wt%) | | | | | −1.9547 | 0.3568 | |
| | MgO melt (wt%) | | | | | −2.9235 | 0.6803 | |

Table 4 (*continued*)

| | AR-IV | *Y* intercept | Standard error *Y* | $R^2$ | *N* | Slope *X* | Standard error *X* | Eq. # |
|---|---|---|---|---|---|---|---|---|
| *RT* ln *D* Gd | | −80.023 | 14.992 | 0.9059 | 8 | (SE = 3.4775) | | 47c |
| | $SiO_2$ melt (wt%) | | | | | 0.9450 | 0.18446 | |
| | Molar An | | | | | −20.605 | 11.039 | |
| *RT* ln D Tb | | −28.322 | 20.464 | 0.7588 | 24 | (SE = 4.4583) | | 48c |
| | $SiO_2$ melt (wt%) | | | | | 0.2452 | 0.25289 | |
| | Molar An | | | | | −31.058 | 10.052 | |
| *RT* ln D Dy | | −69.685 | 16.4202 | 0.8400 | 28 | (SE = 4.3268) | | 49c |
| | $SiO_2$ melt (wt%) | | | | | 0.7924 | 0.19124 | |
| | Molar An | | | | | −27.132 | 8.9685 | |
| *RT* ln *D* Y | | −118.14 | 20.154 | 0.6451 | 48 | (SE = 8.4119) | | 50c |
| | $SiO_2$ melt (wt%) | | | | | 1.3274 | 0.24103 | |
| | Molar An | | | | | −2.1499 | 9.8457 | |
| Element | | | | | | | | |
| *RT* ln *D* Er | | −79.808 | 21.351 | 0.6780 | 15 | (SE = 6.8359) | | 51c |
| | $SiO_2$ melt (wt%) | | | | | 0.8502 | 0.26630 | |
| | Molar An | | | | | −25.099 | 13.1236 | |
| *RT* ln *D* Yb | | −61.048 | 36.287 | 0.3428 | 40 | (SE = 12.1524) | | 52c |
| | $SiO_2$ melt (wt%) | | | | | 0.5258 | 0.42449 | |
| | Molar An | | | | | −18.441 | 18.598 | |
| *RT* ln *D* Lu | | −94.967 | 16.727 | 0.8798 | 17 | (SE = 4.5191) | | 53c |
| | $SiO_2$ melt (wt%) | | | | | 1.0730 | 0.18344 | |
| | Molar An | | | | | −16.526 | 12.233 | |
| *RT* ln *D* Nd | $H_2O$ (wt%) | −20.625 | 6.3101 | 0.2280 | 28 | 5.4674 | 1.9728 | 44e |
| *RT* ln *D* Y | $H_2O$ (wt%) | −28.386 | 12.660 | 0.0798 | 44 | 2.5509 | 1.3368 | 50e |
| ln *D* La | *T* (°C) | −2.2695 | 0.29372 | 0.0288 | 26 | 0.000415 | 0.000492 | 54 |
| ln *D* Ce | *T* (°C) | −1.9980 | 0.28792 | 0.0003 | 25 | −0.00004 | 0.000486 | 55 |
| ln *D* Nd | *T* (°C) | −2.3058 | 0.38069 | 0.0052 | 23 | 0.000214 | 0.000646 | 56 |
| ln *D* Sm | *T* (°C) | −3.5171 | 0.48943 | 0.0635 | 24 | 0.001015 | 0.000831 | 57 |
| ln*D* Y | *T* (°C) | −6.6560 | 0.64144 | 0.1083 | 18 | 0.002721 | 0.001952 | 58 |
| ln *D* Yb | *T* (°C) | 1.9562 | 0.40171 | 0.7232 | 13 | −0.006125 | 0.001142 | 59 |
| *Regression constants*[a] | | | | | | | | |
| *RT* ln *D* B | An | 9.9 | 3.8 | | | −0.61 | 0.5 | 61[a] |
| *RT* ln *D* F | An | 23.6 | 7.1 | | | −37.8 | 11.5 | 62[a] |
| *RT* ln *D* Cl | An | 11.0 | 5.3 | | | −24.5 | 9.5 | 63[a] |
| Polynomial regression : $N = 17$ | | | $R^2 = 0.5607$ | | | | | 46d |
| $RT \ln D\ \mathrm{Eu} = -45.110 + (-5.2769 \log f_{O_2} + (-0.1400\ (\log f O_2)^2)$ | | | | | | | | |
| | | ±21.987 | ±3.9456 | ±0.1690 | | | | |

| | Average *D* | Standard deviation | *N* | Source |
|---|---|---|---|---|
| Sb | 0.2686 | 0.1366 | 3 | (4,7) |
| Mo | 0.39 | — | 1 | (d1) |
| As | 0.2491 | 0.1420 | 3 | (7) |
| Re | 0.01 | | 1 | (R) |
| Ru | <0.3 | | 1 | (c3) |
| Rh | <0.4 | | 1 | (c3) |
| Pd | <0.2 | | 1 | (c3) |

Average values are given where data were inadequate to allow regression. Values of regression constants for *D* F, *D* Cl, *D* Li and *D* B are from Bindeman et al. (1998). Estimates of the errors on the regressions and the fit ($R^2$) are also given.

[a] From Bindeman et al. (1998).

these equations, values of *D* REE-Y can then be calculated with the Lattice Strain Model, and combined with the other regressions, in order to generate a composite parameterization that is consistent with theory, which can easily be integrated into existing spreadsheets and modeling algorithms, and that applies to a wide range of melt compositions (Fig. 16).

## 2. Results

### 2.1. Plagioclase An-content vs. temperature, pressure, and melt composition

Both plagioclase An-content and temperature are needed to calculate the partition coefficients using Eq. (A).

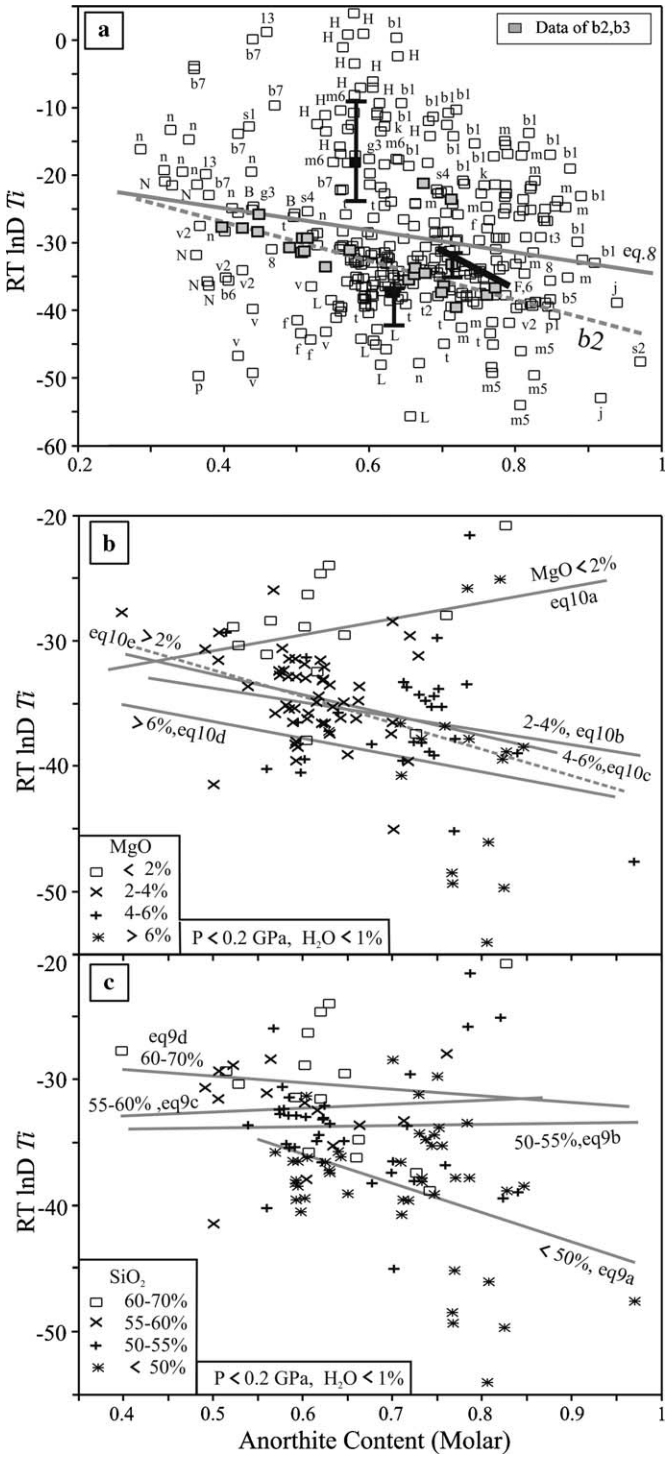


Fig. 3. (a) $RT \ln D$ Ti plotted against plagioclase anorthite content. Note the extensive scatter. Experimental and natural data are not distinguished here. There are very few natural data, and they all fall in the main cluster. Temperatures for natural data were calculated from Eq. 5, Table 2. The dashed line labelled 'b2' is from Bindeman et al. (1998). The unlabelled grey line is Eq. 8 from Table 3. The heavy black line labelled 'F,6' shows how $RT \ln D$ Ti varies with An-content for the Ferrar dolerites as calculated from Eq. 6. A subset of low-pressure dry experimental data were binned into restricted (b) MgO (Eq. 10, Table 3), and (c) $SiO_2$ ranges (Eq. 9, Table 3); showing how $RT \ln D$ Ti generally increases as MgO drops and $SiO_2$ increases.

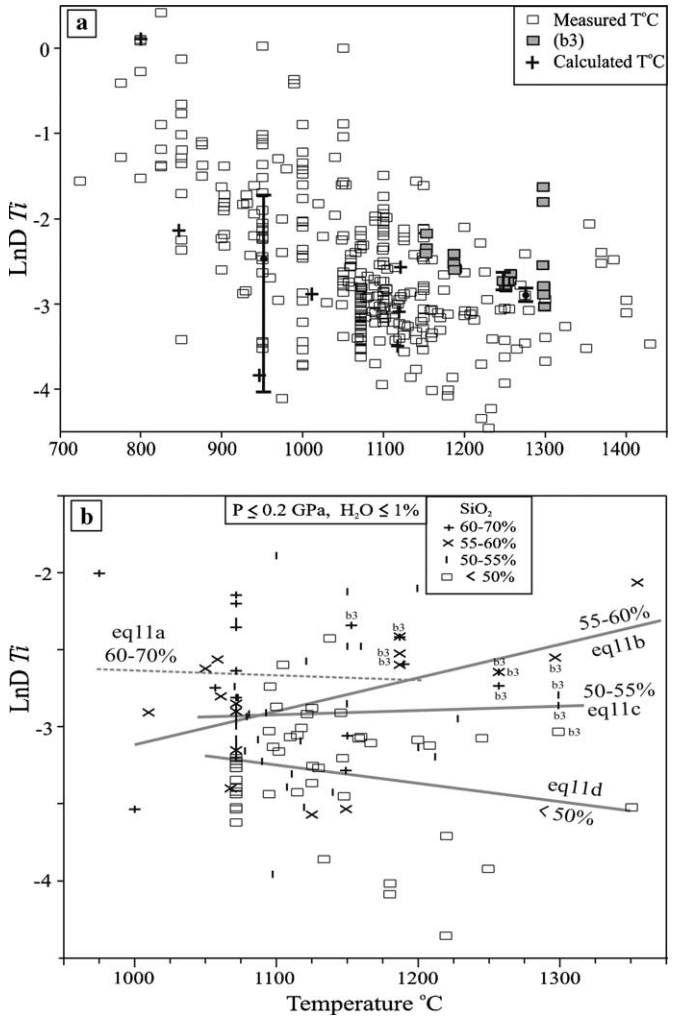


Fig. 4. (a) $\ln D$ Ti plotted against temperature (°C). All of the low-pressure dry experimental data are shown, suggesting a trend of increasing $\ln D$ Ti as temperature drops. Temperatures for natural data were calculated from Eq. 5, Table 2. Ion probe data from Bindeman and Davis (2000, b3) are shown as shaded boxes. Note that these data show the same scatter as electron probe data. In (b) data are binned into restricted compositional ranges (Eq. 11, Table 3). Note that once the compositional effect is removed by binning, most data show no significant trend with cooling.

In ideal circumstances, both can be independently constrained, allowing an unique solution. However, in many cases one or both of these parameters are unknown, and it would be useful to derive expressions allowing them to be calculated if necessary. Plagioclase An-content tends to decrease as magmas cool and evolve (Bowen, 1928). However, plots of plagioclase An-content against temperature show considerable scatter (Fig. 1a), especially for hydrous melts, indicating that other factors than temperature are also important. Several studies have shown that pressure, melt composition and melt water content affect plagioclase An-content (Housh and Luhr, 1991; Panjasawatwong et al., 1995; Takagi et al., 2005). Both Panjasawatwong et al. (1995) and Takagi et al. (2005) provide equations linking plagioclase An-content to tempera-

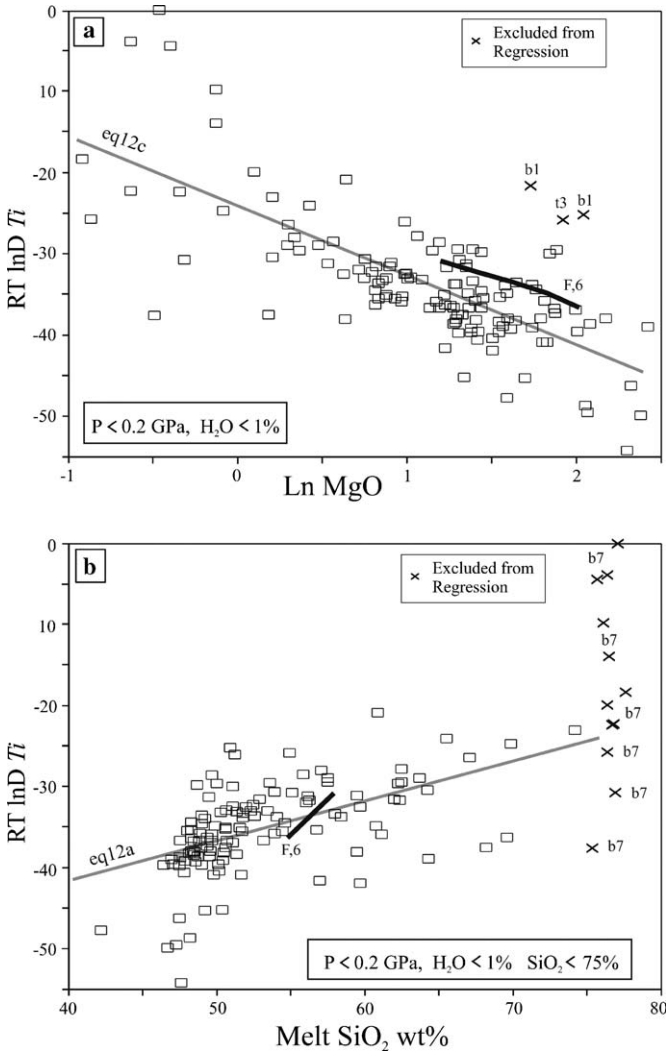


Fig. 5. (a) $RT \ln D$ Ti plotted against lnMgO (Eq. 12c, Table 3), and (b) $SiO_2$ (Eq. 12a, Table 3) in the melt, for low-pressure dry experiments. Temperatures for natural data were calculated from Eq. 5, Table 2. The heavy black lines labelled 'F,6' show how $RT \ln D$ Ti varies for the Ferrar dolerites as calculated from Eq. 6.

ture and melt composition (Eqs.1 and 2, Table 2), but these equations only apply to a limited compositional range, and it would be useful to derive an equation of more general applicability. Fig. 1b and c show that An-content is reasonably well correlated against the MgO or lnMgO content of the melt. The regression coefficients of Table 2 (Eq. 3) can be used to link An-content to melt MgO for wet and dry systems. A multiple regression analysis of this dataset was performed against temperature, pressure, water content and melt MgO content (Eq. 4, Table 2) and yields a more accurate value of the An-content (Fig. 1d). Melt lnMgO content is plotted against inverse temperature for wet and dry systems in Fig. 2a and b. The dry data appear to define a dog-leg, but this may be an artefact caused by a lack of data for cooler melts. If a few outliers are excluded, then all of the data can be regressed together (Eq. 5, Table 2), allowing melt temperature to be calculated from the melt MgO content for any plagioclase-saturated system (Fig. 2c).

These expressions (Table 2) may be useful in a number of ways. For example, they allow plagioclase composition to be calculated in metavolcanic rocks if melt MgO content can be estimated from whole-rock or melt inclusion analyses. Conversely, if only the An-content of the feldspar can be analyzed directly (restites or cumulates), then these expressions allow melt MgO content and temperature to be estimated.

### 2.2. $^{Plagioclase/melt}D$ Ti

Data for $D$ Ti is extensive. Plots of $RT \ln D$ Ti against plagioclase An-content show a diffuse trend of increasing $D$ Ti as An-content decreases (Fig. 3a). The ion-probe $D$ Ti data of Bindeman et al. (1998, b2) and Bindeman and Davis (2000, b3) are distinguished on some of the figures to highlight potential differences between electron- and ion-probe data. Although in most cases the dedicated ion-probe $D$ Ti data appears better behaved than the more diffusely correlated electron-probe data (e.g. Figs. 3 and 4), some of the ion-probe $D$ Ti determinations also plot apart from the main trend. All of the data were regressed together (Fig. 3a, Eqs. 7 and 8, Table 3), yielding a slightly shallower trend than that proposed by Bindeman et al. (1998). Nevertheless, the fit is poor, and other input variables must also be considered for their impact on $D$ Ti variations.

Plots of $\ln D$ Ti vs. temperature show an overall increase of $D$ Ti as temperature drops (Fig. 4a). Typical error estimates are shown for an ion-microprobe analysis from Bindeman et al. (1998, b2, 5% relative) and two phase equilibrium studies where $TiO_2$ was analyzed with the electron microprobe. Uncertainty in temperature is smaller than the symbol size. The datum at 1275 °C from Longhi et al. (1999) shows a restricted $D$ Ti uncertainty that reflects the low analytical error of this study ($TiO_2$ melt $1.09 \pm 0.04$, $TiO_2$ plagioclase $0.06 \pm 0.01$). The uncertainty on this electron probe analysis is comparable to that of the ion-microprobe data from Bindeman et al. (1998) and Bindeman and Davis (2000). Note also that the ion-microprobe data (shaded boxes in Fig. 4a) show a distribution roughly parallel to the main trend of the data, and show similar absolute variations of $\ln D$ Ti for a given temperature. The electron-probe datum at 951 °C from Martel et al. (1999) has a greater uncertainty that reflects a lower precision, the result mainly of lower abundances ($TiO_2$ melt $0.48 \pm 0.09$, $TiO_2$ plagioclase $0.04 \pm 0.03$).

To establish a baseline from which variations of $D$ Ti against changes of $P$–$T$–$X$ can be understood, a subset of data for dry ($H_2O < 1\%$), low-pressure ($P < 0.2$ GPa) experiments was binned for melt $SiO_2$ content and plotted against experimental temperature (Fig. 4b). The data from Bindeman and Davis (2000, b3) appear to define a trend of increasing $\ln D$ Ti as temperature drops (Fig. 4a), but the lower $\ln D$ Ti values correspond to low-$SiO_2$ melts and high-An feldspars, while the high $\ln D$ Ti values correspond to high-$SiO_2$ melts and low-An feldspars; so that it is not possible to discriminate between temperature,

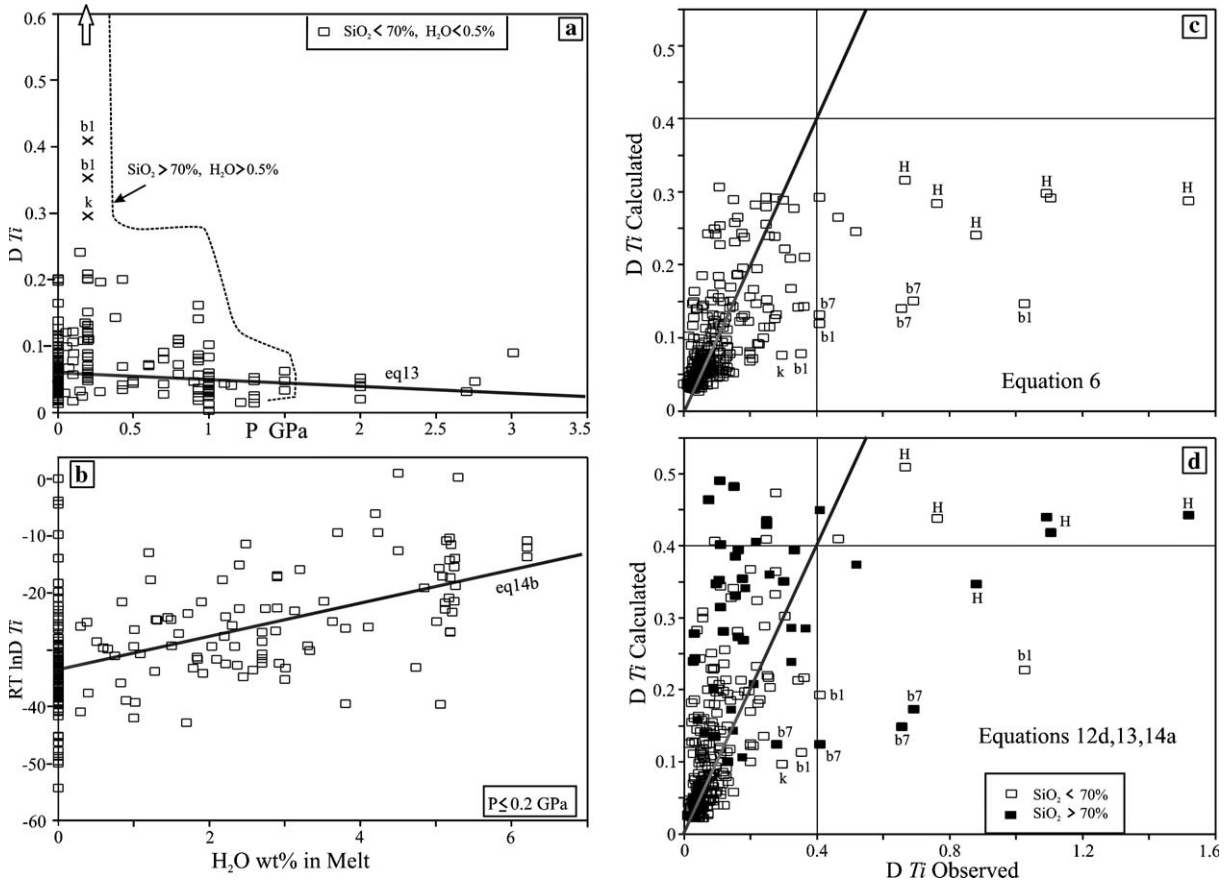


Fig. 6. (a) *D* Ti plotted against pressure in GPa (Eq. 13, Table 3, 3 data excluded (X) from regression), and (b) $RT \ln D$ Ti plotted against wt% melt $H_2O$ (Eq. 14b, Table 3). Only experimental data are shown in (a). Comparison between observed *D* Ti and *D* Ti calculated using: (c) Eq. 6 (Table 3) and (d) Eq. 12d corrected for pressure and water content using the slopes of Eqs. 13 and 14a.

crystal chemistry, and melt compositional effects without considering the entire dataset. In contrast to the overall trend of increasing $\ln D$ Ti with decreasing temperature (Fig. 4a), the binned data either show no trend, or very poorly defined trends of decreasing or increasing $\ln D$ Ti as temperature drops (Fig. 4b, Eqs. 11, Table 3: note the very low $R^2$ values). This implies that temperature variations alone cannot account for the overall $\ln D$ Ti increase seen in Fig. 4a. What is apparent from Fig. 4b, however, is that most $\ln D$ Ti values increase systematically from melts with $SiO_2 < 50\%$ to melts with $SiO_2 > 60\%$. This implies that the observed increase in $\ln D$ Ti has more to do with increasing melt $SiO_2$ than decreasing temperature. In Fig. 5, *D* Ti data ($RT \ln D$ Ti) from low-pressure, dry experiments ($H_2O < 1\%$, $P < 0.2$ GPa) were plotted against melt $SiO_2$ and MgO contents, showing clear trends of increasing *D* Ti as melts evolve (Eqs. 12, Table 3). However, since changes in melt composition are intimately linked to changes in plagioclase An-content, a test is required to clarify the relative influences of melt vs. crystal chemistry. To this end, the same low-pressure, dry subset of *D* Ti data ($H_2O < 1\%$, $P < 0.2$ GPa) was binned for different $SiO_2$ and MgO ranges and plotted against An-content (Fig. 3b and c), to help determine whether the increase in D *Ti* is primarily due to changes in An-content or to melt compositional effects. As in Fig. 4b, the values of $RT \ln D$ Ti for more evolved melts consistently fall above those of more primitive melts (Fig. 3b and c), suggesting an important melt compositional control. However, many of the binned data also show trends of increasing $RT \ln D$ Ti as An-contents decrease (Eqs. 9 and 10, Table 3), which implies that there is also a crystal-chemical control.

If data from the most evolved (>70% $SiO_2$) and wettest (>5% $H_2O$) compositions are excluded, then plots of *D* Ti and $RT \ln D$ Ti vs. pressure (Fig. 6a) show a diffuse trend of *D* Ti decrease as pressure increases (Eq. 13, Table 3), with changes in the order of 0.01/GPa. If only low-pressure data are considered, then plots of $RT \ln D$ *Ti* and *D* Ti vs. melt $H_2O$ (Fig. 6b) both show clear trends of increase as melt $H_2O$ increases (Eq. 14), with *D* Ti increasing by about 0.027/wt% $H_2O$ in the melt. Most of the data for melt $H_2O$ contents was calculated by the difference method (100% minus analytical total), however, and is rather imprecise in consequence. The slopes of Eqs. 13 and 14 can be used in tandem with the simplified equations for variations of low-pressure anhydrous *D* Ti (or $RT \ln D$ Ti) linked to changes of melt composition

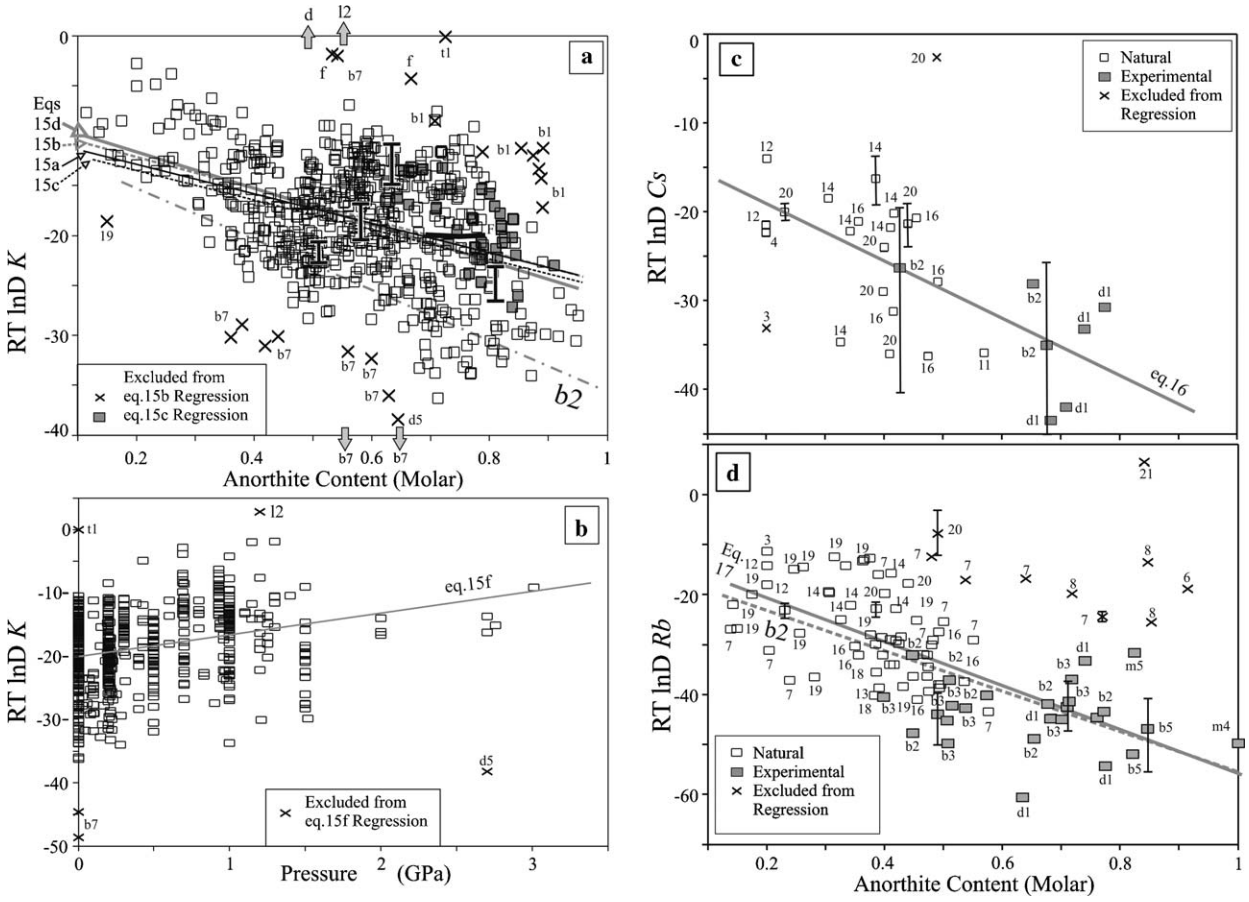


Fig. 7. (a) $RT \ln D$ K plotted against plagioclase anorthite content. The regression results of Bindeman et al. (1998) are shown as a dash-dot line labelled 'b2'. The other regressions are labelled according to the equations in Table 4. The heavy black line labelled 'F' shows how $RT \ln D$ K varies for the Ferrar dolerites as calculated from Eq. 15h. (b) $RT \ln D$ K plotted against pressure in GPa. (c) $RT \ln D$ Cs, and (d) $RT \ln D$ Rb plotted against plagioclase anorthite content. In (c) the grey line is the regression from this paper (Eq. 16, Table 4). In (d) the Bindeman et al. (1998) regression is labelled 'b2,' while the grey line is the regression from this paper (Eq. 17, Table 4). Representative error bars are shown.

or An-content (Eqs. 9, 10 or 12) to obtain a more precise estimate of $D$ Ti if the pressure and water content of the melt are known. Variations of similar extent might be expected for other high-charge cations, such as the rare earth elements.

Multiple regression analysis implies that the dominant causes of variation of $\ln D$ Ti are melt $SiO_2$, melt MgO, and pressure; with temperature, water-content and plagioclase An-content being of secondary importance (Eq. 6, Table 3). The multiple regression results (Fig. 6c, Eq. 6, Table 3) fit much (but not all) of the data reasonably well ($R^2 = 0.4939$), but there are serious discrepancies for some data (notably those from H, b7 and b1). Removal of these three datasets did not significantly improve the regression results, however. It is worth pointing out that the fit for low-pressure anhydrous data ($RT \ln D$ Ti) calculated from ln MgO ($R^2$ of 0.5533, Eq. 12c) is as good as the multiple regression analysis; and if the value of $D$ Ti calculated from Eq. 12c is corrected for pressure and water content using the slopes of Eqs. 13 and 14a, the correlation with observed data is no worse than those of the multiple regression analysis for mafic melts (compare Fig. 6c and d).

To summarize: $D$ Ti variations are complex functions of plagioclase composition (An), pressure, temperature, and melt composition ($H_2O$, MgO, and $SiO_2$ contents); which are only partly captured by the regression analysis. In practical terms, a straightforward way to approximate the $D$ Ti value for the system of interest might be as follows:

(A) For well constrained environments, use the multiple regression analysis (Eq. 6).
(B) For poorly constrained scenarios, use the regressions based on melt lnMgO or $SiO_2$ (Eq. 12), and correct for pressure and $H_2O$ content using Eqs. 13 and 14a.

### 2.3. Large ion lithophile elements (LILE) and alkaline earths: K, Cs, Rb, Ba, Sr, Pb, Li

The dataset for $D$ K is very large because of the incorporation of data from phase equilibrium studies (Fig. 7a). Values of $RT \ln D$ K increase as An decreases (Fig. 7a), but results are scattered, despite fairly restricted 1-σ error estimates on most data. The regres-

sion of Bindeman et al. (1998, b2) under-estimates most existing $D$ K values (Fig. 7a), while a regression on all data (Eq. 15a, Table 4) has a slope that is slightly too shallow to reproduce many data from very felsic or mafic melts. As a palliative, the extreme outliers were excluded (Eq. 15b, 'X' symbols on Fig. 7a), the same outliers as well as the data from 'b1' were excluded (Eq. 15c, shaded boxes on Fig. 7a), and only low-pressure data were regressed (Eq. 15d). All results are similar, however, with the best statistics being those of Eq. 15c. A scattered trend of increasing $RT \ln D$ K as $P$ increases is also seen (Fig. 7b). Multiple regression analysis implies a significant role for An-content, pressure and for melt MgO and $SiO_2$ contents, and yields the best (although still poor) fits ($R^2 = 0.3042$, Eq. 15h, Table 4).

Data for $D$ Cs is scanty, and two older data were excluded (Eq. 16, Fig. 7c). The new $D$ Rb regression (Eq. 17) closely resembles that of Bindeman et al. (1998) if a few outliers are excluded (Fig. 7d). Data for $D$ Pb are scattered (Fig. 8b); and the new regression (Eq. 20) is significantly shallower than that of Bindeman et al. (1998). An 0.05 decrease of $D$ Pb for each % $H_2O$ in the melt was observed (not shown). Data for $D$ Li scatter widely and yield only a poorly constrained regression against An-content (Eq. 21, Table 4).

Values of $RT \ln D$ Ba show systematic increases with increasing contents of An, melt $SiO_2$, and with decreasing melt MgO. There are too few high-pressure data to allow this variable to be evaluated, while variations in water content are unsystematic. The equations of Blundy and Wood (1991) and Bindeman et al. (1998) both provide reasonably good fits to the expanded database. A regression for $RT \ln D$ Ba (Eq. 18a, Fig. 8a) yields a trend slightly shallower than those proposed by Blundy and Wood (1991, BW) and Bindeman et al. (1998, b2). This regression (Eq. 18a) excludes a few of the worst outliers, notably, many data from Luhr and Carmichael (1980, 11) plot systematically low, for unknown reasons. Multiple regression analysis of the $RT \ln D$ Ba data (excluding the same outliers shown on Fig. 8a) yields a slightly more precise estimate of $D$ Ba (Eq. 18b).

There are enough $D$ Sr data to allow several potential input variables to be considered. Values of $RT \ln D$ Sr show systematic increases with increasing contents of An, of melt $H_2O$ and $SiO_2$, with decreasing melt MgO, and with decreasing pressure. High-pressure data are largely from Van der Auwera et al. (2000, v), with one datum from Blundy et al. (1998, b6). If one outlier from 'v' is excluded, and low-pressure data between An contents of 40 and 70 are averaged to anchor the trend, then regressions against pressure (Eqs. 19b and c) imply that $D$ Sr decreases by about 1.4 D for each increase of 1 GPa. In contrast, values of $D$ Sr increase by about 1.5 D/% $H_2O$ in the melt (Eqs. 19d and e).

If low-pressure (<1.3 GPa), low-$H_2O$ (<3%) data only are considered, and a few outliers are excluded, then a regression for $RT \ln D$ Sr (Eq.19a) yields a trend only slightly shallower than those proposed by

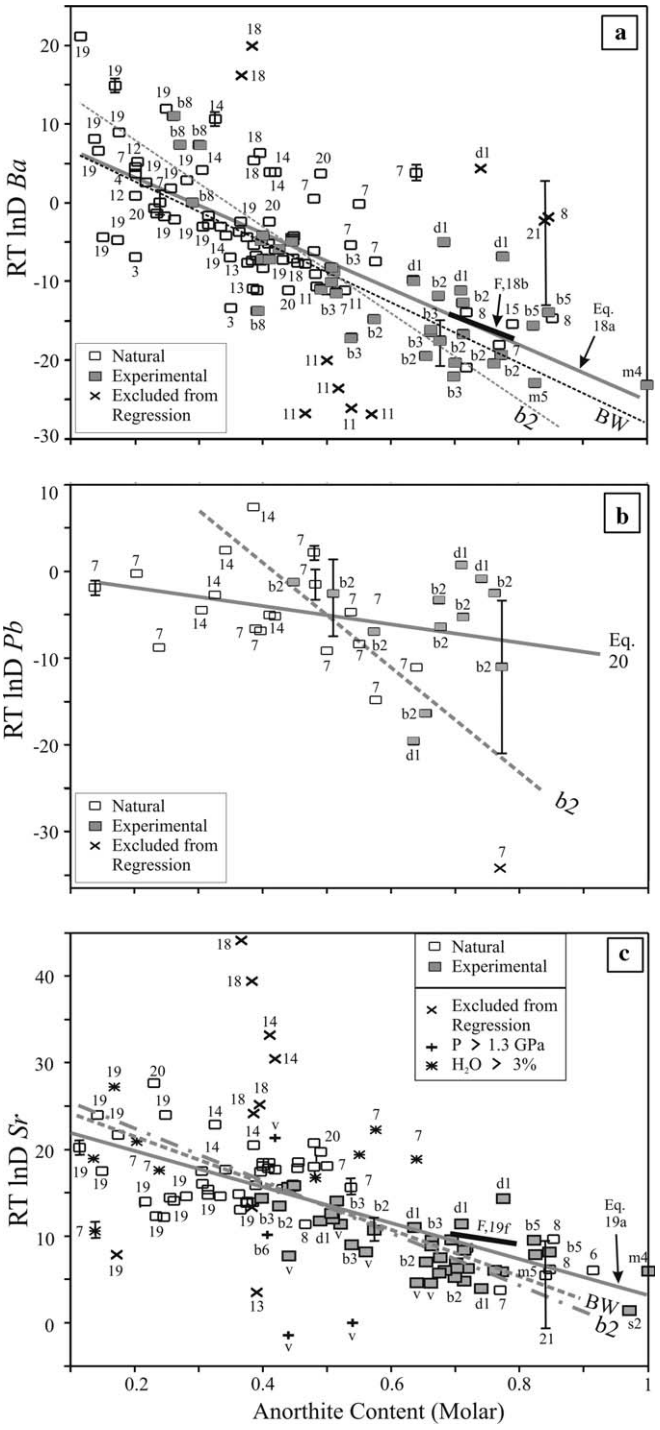


Fig. 8. (a) $RT \ln D$ Ba, (b) $RT \ln D$ Pb, and (c) $RT \ln D$ Sr plotted against plagioclase anorthite content. The regression results of Bindeman et al. (1998) are shown as a dash-dot lines labelled 'b2'. The dashed lines labelled 'BW' are regressions proposed by Blundy and Wood (1991). The continuous grey lines are regression results from this paper (Table 4). Error bars show 1-σ error estimates. The heavy black lines labelled 'F,18b' (in a) and 'F,19f' (in c) show how $RT \ln D$ Ba and Sr vary for the Ferrar dolerites as calculated from Eqs.18b and 19f, respectively.

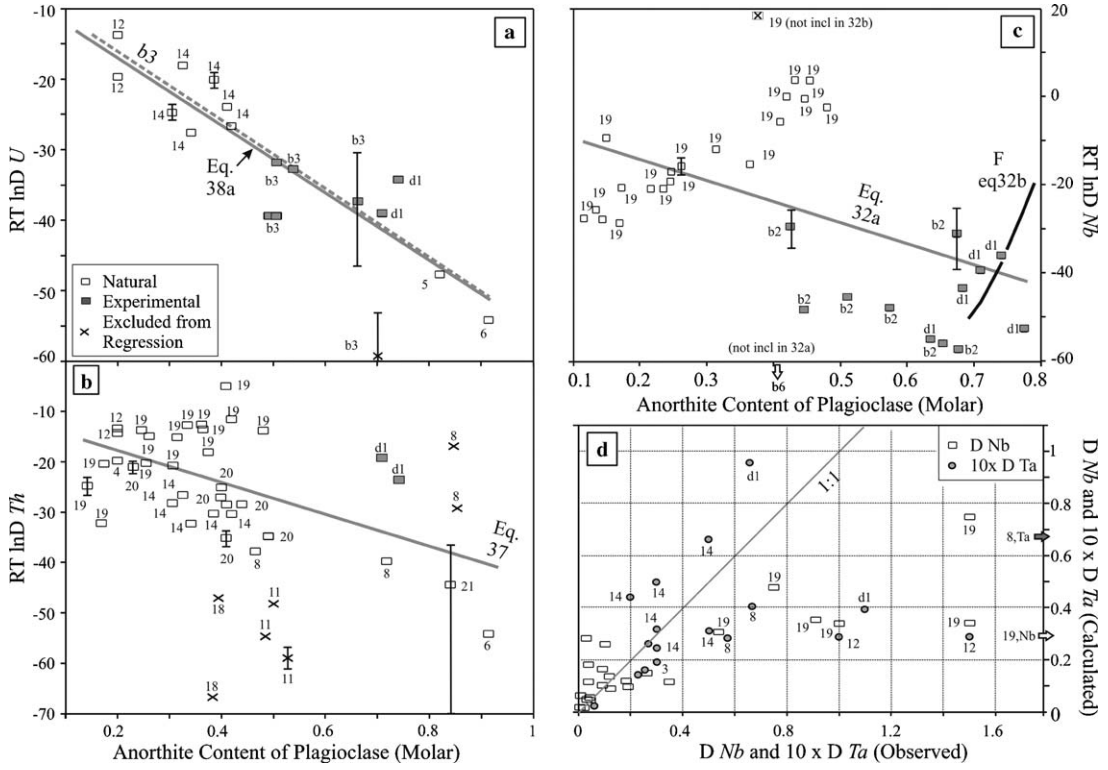


Fig. 9. (a) $RT \ln D$ U, (b) $RT \ln D$ Th, and (c) $RT \ln D$ Nb plotted against plagioclase anorthite content. The regression results of Bindeman et al. (1998) are shown as a dashed line labelled 'b2.' The continuous grey lines are regression results from this paper (Eqs. 37, 38a, 32a, Table 4). The heavy black line labelled 'F,eq32b' shows how $RT \ln D$ Nb varies for the Ferrar dolerites as calculated from Eq. 32b. Note that the Ferrar trend (in c) is at a sharp angle to the trend calculated from the An-content. (d) Compares calculated values of $D$ Nb (eq.32b) and $10 \times D$ Ta (Eq. 33) with observed values.

Blundy and Wood (1991, BW) and Bindeman et al. (1998, b2) (Fig. 8c). This regression (Eq. 19a) excludes data from Wörner et al. (1983, 18), since these may very well be from high-pressure hydrous melts. A topaz rhyolite 98,702 from Ren et al. (2003, 19) also falls off the main trend, possibly due to anomalous enrichment in halogens? Data for two granites from Nash and Crecraft (1985, 14) and a rhyolite from Nagasawa and Schnetzler (1971, 13) also fall off the main trend, for unknown reasons. The P- and $H_2O$-corrections (Eqs. 19b–e) can be applied to values of $D$ Sr calculated solely from the low-pressure data (Eqs.19a, f and g). Multiple regression analysis of the $RT \ln D$ Sr data (excluding high-pressure data, and the same outliers as for the Eq. 19a regression) yield reasonably good results (Eqs. 19f and g).

### 2.4. High field strength cations: U, Th, Nb, Ta, P, Zr, Hf, Be

The equations of Bindeman and Davis (2000) fit the available $RT \ln D$ U data well (Fig. 9a), and the new regression (Eq. 38a) differs only slightly from theirs. Data from Michael (1983) were given a temperature appropriate to a melt with 0.2% MgO (755 °C, Eq. 5). Data for $RT \ln D$ Th is scattered (Fig. 9b) with much of the older data plotting off the main trend, so that the derived coefficients (Eq. 37) should be viewed with caution. More experimental $D$ Th data are needed to provide better constraints. Data for $RT \ln D$ Nb (Eq. 32a, Fig. 9c) and $RT \ln D$ Ta (not shown) are poorly correlated with An-content, but seem to yield reasonable fits for multiple regression using melt $SiO_2$, MgO and An-content (Eqs. 32b and 33, Fig. 9d). However, when a trend for $RT \ln D$ Nb is calculated for a specific magmatic suite (e.g. the Ferrar dolerites, 'F Eq. 32b' in Fig. 9c), the variation is at a sharp angle to the overall trend. Because of the weights given to the different input parameters by the multiple regression analysis, $D$ Nb and $D$ Ta both seem to go through a minimum for intermediate melt compositions. More experimental data for $D$ Nb and $D$ Ta are needed to clarify how $D$s vary.

Data for $D$ P are scanty (not shown). Most of the $D$ P data from Gerke et al. (2005), Toplis and Carroll (1995) and Toplis et al. (1994) scatter with no obvious trend, and were excluded from the regression. The best behaved data are those of Bindeman et al. (1998), Bindeman and Davis (2000), and Tuff et al. (2005); and the regression obtained (Eq. 39) differs only slightly from previous estimates. Data for $D$ Be are mostly from Bindeman et al. (1998) and Bindeman and Davis (2000), and the new regression (Eq. 22) differs only slightly from theirs. Unusually, $D$ Be decreases as An-content drops.

Plots of $RT \ln D$ Zr against An-content show considerable scatter (Fig. 10a). Much of the data of Ewart and Griffin (1994, 7) plots above the other data, suggesting a

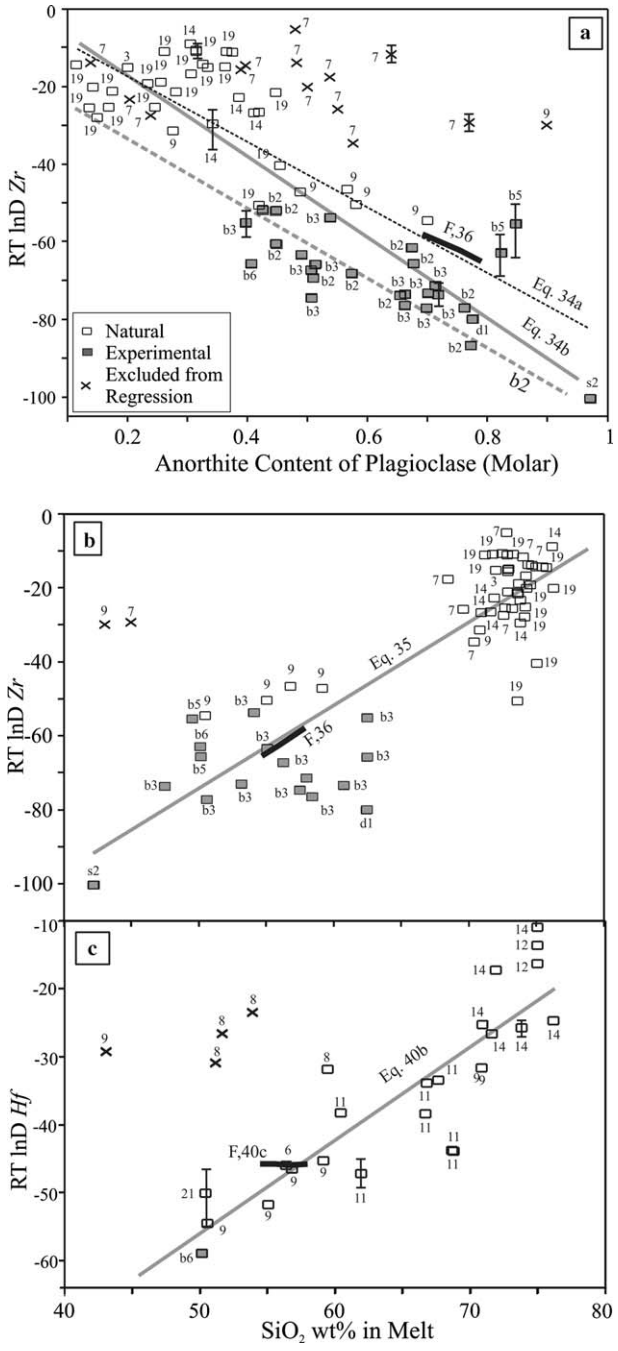


Fig. 10. *RT* ln *D* Zr plotted against plagioclase anorthite content (a) and melt $SiO_2$ content. The regression results of Bindeman et al. (1998) are shown as a dashed line labelled 'b2' (in a). The grey and dotted lines show results from this paper (Eq. 34a from An all data; 34b from An, filtered data; 35 from melt $SiO_2$ content). The heavy black lines labelled 'F,36' (in a and b) show how *RT* ln *D* Zr varies for the Ferrar dolerites. (c) *RT* ln *D* Hf plotted against melt $SiO_2$ content. The grey line shows results from this paper (Eq. 40b, Table 4), with the heavy black line labelled 'F,40c' showing how *RT* ln *D* Hf varies for the Ferrar dolerites.

potential analytical problem. An ugandite from Fujimaki et al. (1984, 9) also plots apart and was excluded. The filtered regression (Eq. 34b) fits the data much better than that calculated from all of the data (Eq. 34a). The equation of Bindeman et al. (1998, b2) underestimates *D* Zr for most felsic data. A regression of *RT* ln *D* Zr against melt $SiO_2$ content yields a much better constrained trend (Eq. 35, Fig. 10b); with only two data being excluded from this regression, the ugandite from Fujimaki et al. (1984, 9)

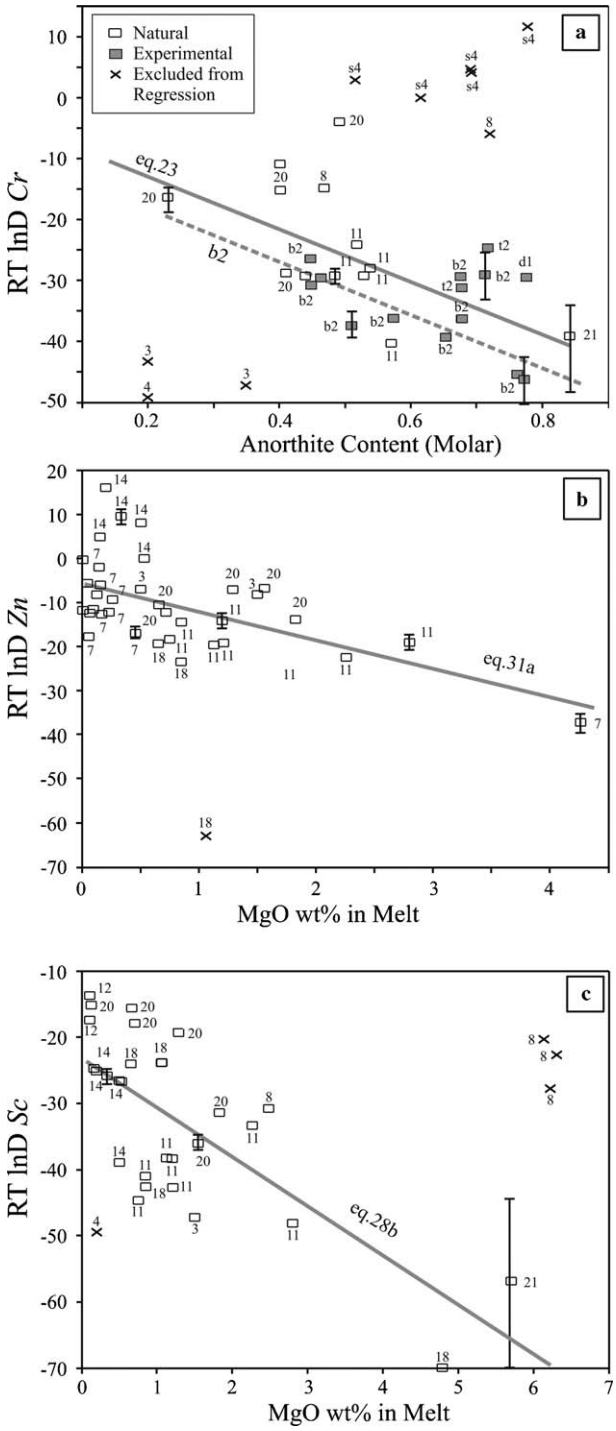


Fig. 11. (a) *RT* ln *D* Cr plotted against plagioclase anorthite content (Eq. 23a, Table 4). (b) Ln *D* Zn (Eq. 31, Table 4), and (c) ln *D* Sc (Eq. 28) plotted against melt MgO content. The regression results of Bindeman et al. (1998) are shown as a dashed line labelled 'b2'. The continuous grey lines are results from this paper.

and a Vesuvius leucitite from Ewart and Griffin (1994, 7). Melt $SiO_2$ content appears to capture most of the variation in $RT \ln D$ Zr; and multiple regression (Eq. 36) shows only modest improvement.

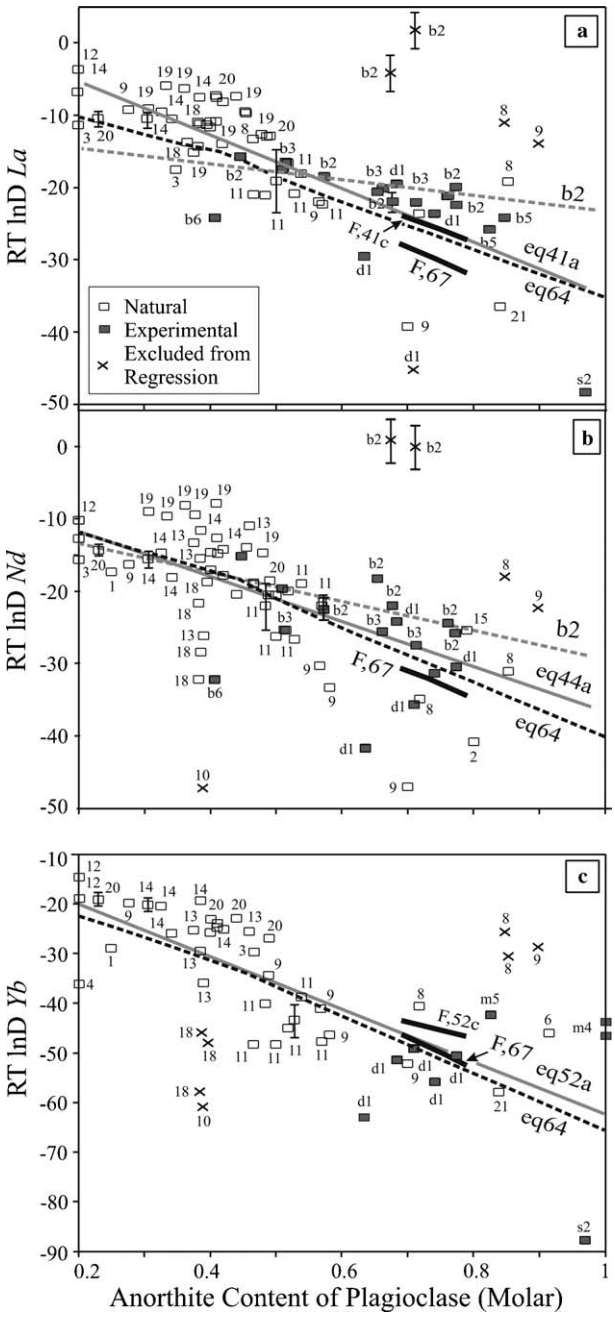


Fig. 12. (a) $RT \ln D$ La, (b) $RT \ln D$ Nd, and (c) and $RT \ln D$ Yb plotted against plagioclase anorthite content. The regression results of Bindeman et al. (1998) are shown as a dashed line labelled 'b2'. The continuous grey lines are regression results (from An) from this paper (Eqs. 41a, 44a, 52a). The black dashed lines labelled 'Eq. 64' shows results of the lattice strain model parameterization calculated from the feldspar An-content (Table 5). The heavy black lines labelled 'F,41c' and 'F,52c' show how $RT \ln D$ La and Yb vary for the Ferrar dolerites as calculated from the multiple regressions (Eqs. 41c and 52c). The heavy black lines labelled 'F,67' are the lattice strain model fits to these regressions. In (b) the regression for $RT \ln D$ Nd (Eq. 44c) is indistinguishable from 'F,67.'

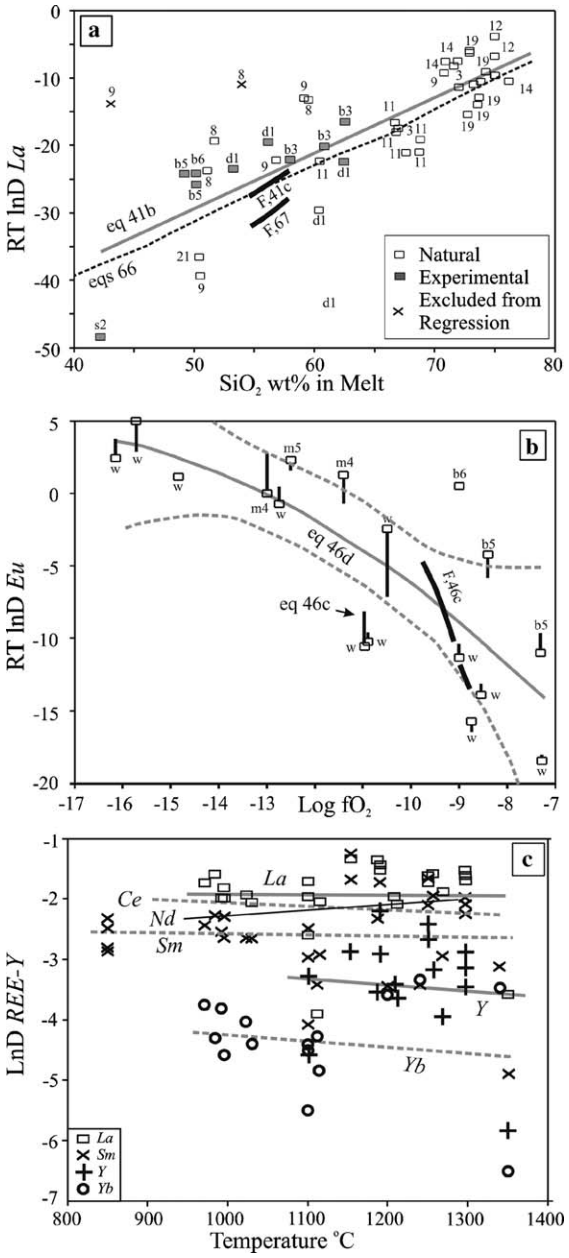


Fig. 13. (a) $RT \ln D$ La plotted against melt $SiO_2$. The continuous grey line is the regression from this paper (Eq. 41b, Table 4). The dashed line labelled 'eqs66' shows the value calculated using the Lattice Strain Model, using the $RT \ln D$ parameterization for melt $SiO_2$ (Eq. 66, Table 5). The heavy black lines labelled 'F,41c' shows how $RT \ln D$ La varies for the Ferrar dolerites as calculated from the multiple regression (Eq. 41c, Table 4). The heavy black lines labelled 'F,67' is the lattice strain model fit to the individual rare earth multiple regressions. (b) $RT \ln D$ Eu plotted against $\log f_{O_2}$. Values of $\log f_{O_2}$ from 'b5' and 'b6' were extrapolated from published values of the buffer curves at higher pressure. The filled grey curve is a polynomial regression (Eq. 46d, Table 4), with the dashed grey curves showing 95% confidence limits. The thick black bars show the difference between the measured values (boxes) and the results of the multiple regression of $RT \ln D$ Eu calculated from melt MgO, melt $SiO_2$, and $\log f_{O_2}$ (Eq. 46c), which appears to be more precise than the polynomial fit to $\log f_{O_2}$ only. The heavy black line labelled 'F,46c' shows how $RT \ln D$ Eu varies for the Ferrar dolerites as calculated from the multiple regression (Eq. 46c, Table 4). In (c) $\ln D$ La–Sm–Y–Yb data for low-pressure, low-$H_2O$ systems only are shown (Eqs. 54–59, Table 4). The data for $D$ Ce and $D$ Nd are not shown. The data show minimal dependence on temperature, with very poor correlations (Table 4).

Data for $RT \ln D$ Hf show a scattered trend of increase as An decreases (Eq. 40a, not shown, calculated excluding: the ugandite from Fujimaki et al. (1984, 9), three data from (Francalanci, 1989, 8), two data from Wörner et al. (1983) and one from Dodge et al. (1982)). A regression of $RT \ln D$ Hf against melt $SiO_2$ content (excluding the same outliers as above) yields a simple linear trend (Eq. 40b, Fig. 10c). The $SiO_2$ contents of the Bishop Tuff samples from Michael (1983, 12) were assumed to be 75%. Melt $SiO_2$ content appears to capture most of the variation in $RT \ln D$ Hf; and multiple regression using melt $SiO_2$ and MgO contents (Eq. 40c) shows only modest improvement.

### 2.5. Metals: Ga, Cr, Ni, Zn, Co, Cu, V, Sc, Ge

Data for $RT \ln D$ Cr are scattered, and the new regression against An-content (Eq. 23, Fig. 11a) differs only slightly from that of Bindeman et al. (1998). For this regression, outliers from (3,4,8,s4) were excluded. Data for evolved melt compositions are scanty, and this part of the compositional spectrum is poorly constrained. $RT \ln D$ Ni increases as An-content decreases, with a single datum from (b2) being excluded from the regression (Eq. 24). $RT \ln D$ Ga shows a diffuse trend of increase as lnMgO decreases (Eq. 25a), $SiO_2$ increases, and as $H_2O$ increases. Trends against An-content are poorly defined (not shown). Multiple regression analysis yields significantly better results for $D$ Ga (Eq. 25b). A single high-pressure determination (b6) is lower than other determinations at a given An-content, suggesting the possibility that $D$ Ga decreases as pressure increases. Sparse $D$ Ge data (Malvin and Drake, 1987) yield a correlation with melt MgO (Eq. 26) strictly only valid between MgO 11 and 16 wt%. Data for $D$ V are sparse, with 4 out of 5 aligning when plotted

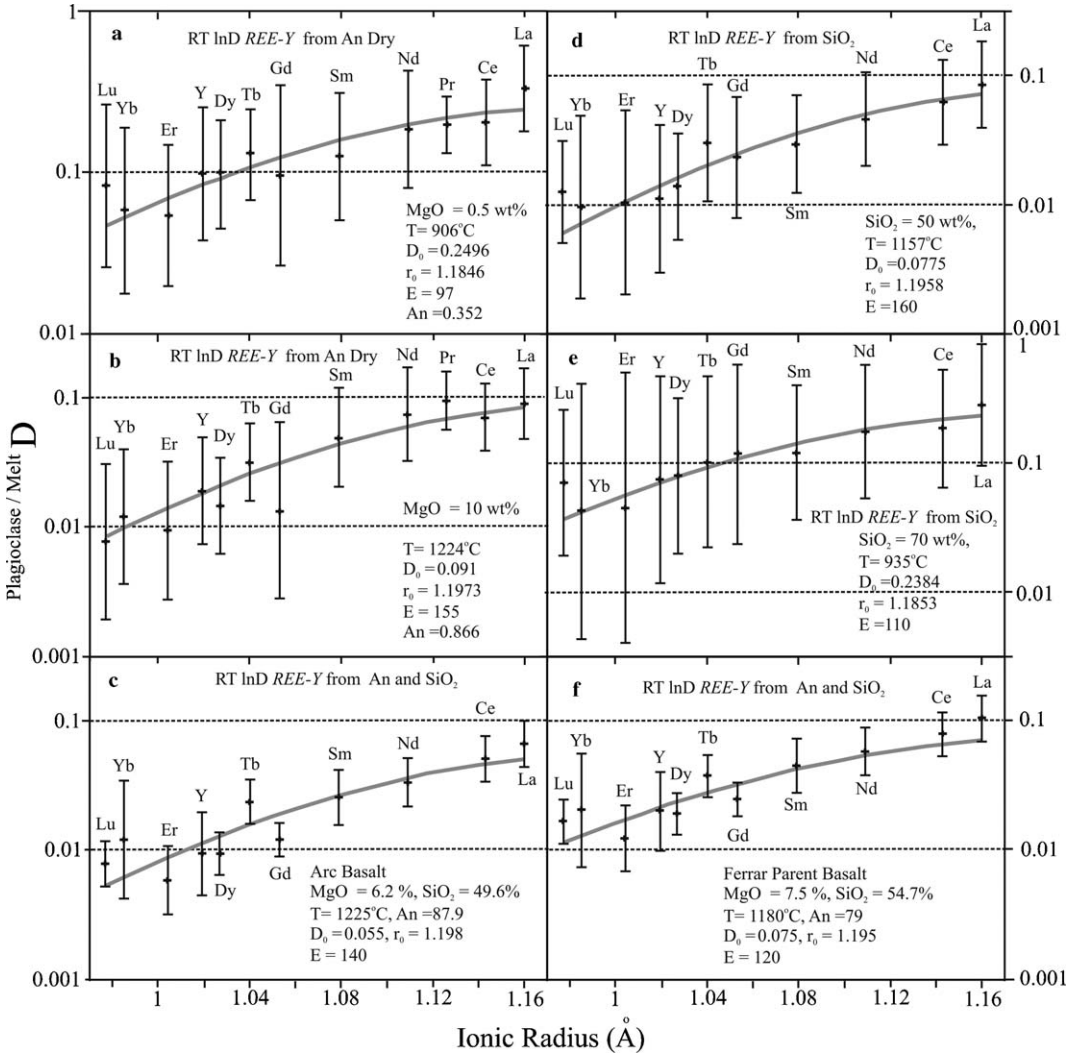


Fig. 14. Values of $D$ REE (rare earth elements) and $D$ Y obtained from the (a and b) regressions of $RT \ln D$ against An-content of plagioclase (dry, Eqs. 3a, 3b, 41a to 53a); (d and e) from regressions of $RT \ln D$ against melt $SiO_2$ (Eqs. 41b–53b); and (c–f) from the multiple regression analysis (Eqs. 41c–53c). $D$ values are plotted against ionic radius (Shannon, 1976). The curves show results of the Lattice Strain Model Eq. (B) fit to these regressions by varying $E$, $D_0$ and $r_0$. Temperature was linked to An-content and/or melt composition using Eqs. 3a, 3b, 5a (a and b); 5b (d and e); or from the PELE simulation results (c and f, see text for details). Values of $D_0$, $E$ and $r_0$ derived by visual fits to the $RT \ln D$ REE-Y regressions were then fit to obtain the parameterization constants of Table 5.

against An-content (Eq. 27, not shown). Data for $RT \ln D$ Sc show a diffuse anticorrelation with melt MgO content (Eq. 28, Fig. 11c), if outliers from Francalanci (1989, 8) and Dodge et al. (1982, 4) are excluded. The anticorrelation of $RT \ln D$ Sc against An is even poorer (not shown), with a trend shallower than that suggested by Bindeman et al. (1998). Two outlying data from (b2) and one from (18) were excluded from the $RT \ln D$ Co regression against An (Eq. 29). $RT \ln D$ Cu increases as MgO and An decrease and $SiO_2$ increases (not shown), with no obvious trend against changing $H_2O$. The best results were obtained from a multiple regression analysis (Eq. 30). However, variations of $D$ Cu are all from a single source (7), and are anchored by a single mafic composition; and should be viewed with caution, especialy for mafic melts. $RT \ln D$ Zn increases as MgO (Eq. 31, Fig. 11b) and An decrease and $SiO_2$ increases, with no obvious trend against changing $H_2O$. A single datum from (18) was excluded from the $RT \ln D$ Zn regression against MgO. Trends of $D$ Zn against An-content are poorly defined (not shown).

### 2.6. Rare-earth elements and yttrium

$RT \ln D$ REE-Y data were regressed against the An-content of plagioclase (Eqs. 41a to 52a, Fig. 12). A datum from Gromet and Silver (1983, 10), data S2-2 and S2-3 from Bindeman et al. (1998, b2), datum 144 from Francalanci (1989, 8) and the ugandite from Fujimaki et al. (1984, 9) were excluded from most regressions because they plotted anomalously. Data for many REE (e.g. $D$ La, Ce, Nd, Sm, Yb, Lu) show moderately good correlations against An-content (Fig. 12). Data for $D$ Eu and Y are also abundant, but are more scattered (not shown). Data for $D$ Gd, Tb, Dy, Tm and Er are sparse, and the high-An end of the spectrum is typically poorly represented (not shown). In some cases the new regressions differ considerably from those of Bindeman et al. (1998) and Bindeman and Davis (2000), showing steeper rates of increase.

Regressions of $RT \ln D$ REE-Y against melt $SiO_2$ (Eqs. 41b to 53b, Table 4, Fig. 13a) and MgO (not shown) contents were also performed, to allow modeling in cases where An-contents cannot be determined. The data show clear trends of increase as melt $SiO_2$ increases and MgO decreases. Where data exists, $D$ REE appear to show trends of increase (as for $D$ Ti) as $H_2O$ content increases (e.g. Eqs. 44e and 50e). The sole high-pressure determination (Blundy et al., 1998, b6) suggests that $D$ REE decrease as pressure increases. More high-pressure data is needed to verify this.

Multiple regressions including combinations of plagioclase An-content and melt $SiO_2$, and $f_{O_2}$ for $D$ Eu, yield the most precise $D$ REE determinations in most cases (Eqs. 41c–53c). Inclusion of melt MgO actually worsens many fits. It is known that $D$ *Eu* varies with changing $f_{O_2}$ conditions (Drake and Weill, 1975; Wilke and Behrens, 1999). Plots of $RT \ln D$ Eu against $\log f_{O_2}$ were fit with a

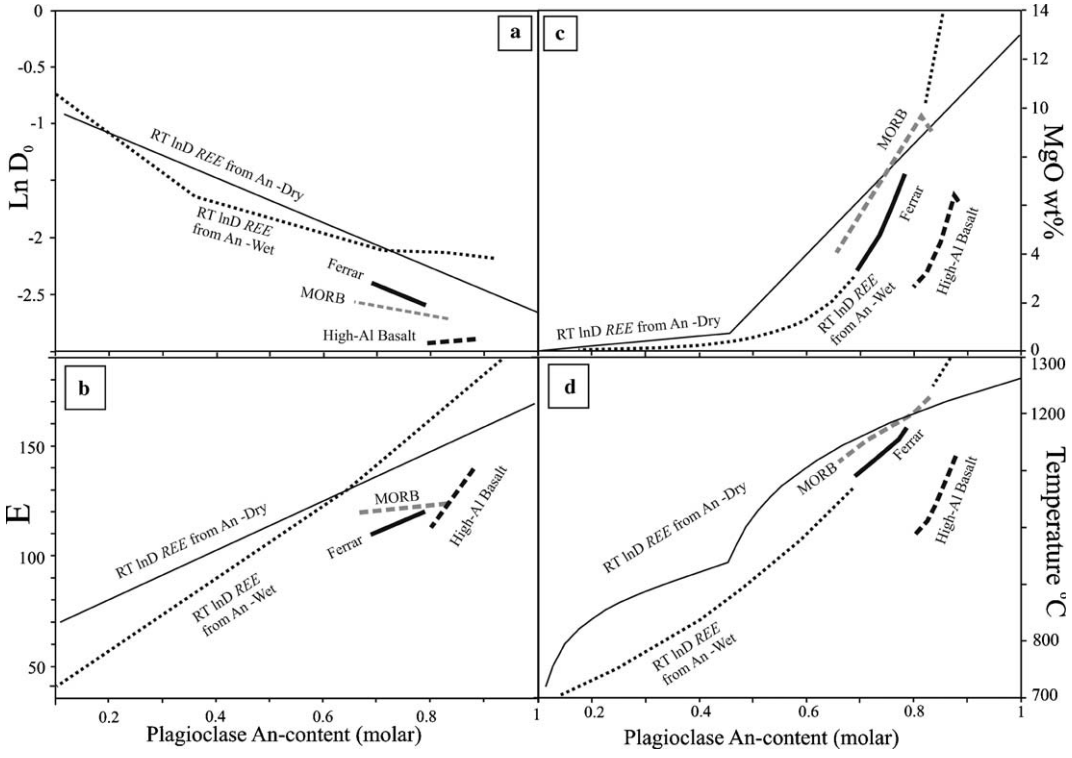


Fig. 15. (a) Ln $D_0$, (b) $E$, (c) melt MgO and (d) temperature variations plotted against plagioclase An-contents; corresponding to the regressions of $RT \ln D$ REE-Y against plagioclase An-contents, for wet and dry systems (Eqs. 64 and 65, respectively, Table 5). Values of $E$ and $\ln D_0$ were derived from fits like those of Fig. 14. Covariations of An-content with melt MgO and temperature for the regressions against An-content are from Eqs. 3a, 3b and 5a (dry system) or 3c and 5a (wet system). The other lines show the trends for the Ferrar (Eq. 64), High-Al arc basalt (Eq. 65) and MORB (Eq. 69) suites calculated in the same way on the basis of PELE simulations (see text).

polynomial function, yielding reasonable fits ($R^2 = 0.5607$, Eq. 46d, Fig. 13b). A multiple linear regression seems to yield a better result, however (Eq. 46c, Fig. 13b). Plots of $\ln D$ REE against temperature show no systematic trend (Fig. 13c), with extremely low $R^2$ (Table 4, Eqs. 54–59), implying that there is little or no temperature effect on REE partitioning.

### 2.7. Other elements

Data for $D$ Sb, Mo, Ru, Rh, Ru, Pd and As are too scattered and sparse to be regressed, and simple averages were computed (Table 4). Data for $D$ B, $D$ F, and $D$ Cl are principally from Bindeman et al. (1998) and Bindeman and Davis (2000), and were not regressed anew. Values of regression constants from these papers for these elements are given in Table 4 for convenience.

## 3. Calculation of $^{\text{plagioclase/melt}}D$ REE-Y profiles and comparison with results of the lattice strain model (LSM)

Values of $D$ REE-Y were calculated from the regressions of $RT \ln D$ REE-Y against An (Table 4), and were plotted against ionic radius (e.g. Fig. 14). Melt MgO and temperature were linked to An-content using Eqs. 3a, 3b and 5a, which are appropriate for dry low-pressure systems. These calculations produce generalized, 'average' magmatic values of $D$ that may be useful when detailed information on melt composition and intensive parameters are lacking. Fig. 14a and b compare values of $D$ REE-Y calculated from the individual dry system regressions of $RT \ln D$ REE-Y against An (Fig. 12), to results of the lattice strain model (LSM) of Blundy and Wood (1991, 1994), also known as the Brice (1975) equation. The LSM posits a parabolic distribution of $D$ values around the ionic radius of the host site $r_0$, which gives the position of the curve apex on the '$x$' (ionic radius) axis. The Blundy and Wood (1994) expression is

$$D_i = D_0 \exp(-4\ \pi\ E\ N_A((r_0/2)\cdot(r_i - r_0)^2 + \frac{1}{3}(r_i - r_0)^3)/RT), \quad \text{(B)}$$

where $D_0$ is the strain compensated partition coefficient, and gives the $D$ value of the curve's apex; $r_i$ is the ionic radius of the cation of interest (Shannon, 1976); $E$ is Young's Modulus of the REE-hosting site, variations of which affects the kurtosis of the model curve; $N_A$ is Avoga-

Table 5
Parameterization for $E$ and $D_0$ vs. MgO or lnMgO (respectively), which feed into the Brice (1975) equation Eq. (B), allowing calculation of $D$ REE and $D$ Y

| Applicable range | Parameter | Calculated from | Intercept $Y$ | Slope $X$ | Eq. # |
|---|---|---|---|---|---|
| $RT \ln D$ REE regressions from An (e.g. $\ln D_0 = X\ \text{An} + Y$) linked to MgO (melt) by Eqs. 3a and 3b, dry system, and T° C by Eq.5a | | | | | |
| An0.1–1 | $\ln D_0$ | An | −0.69478 | −1.9698 | 64a |
| An0.1–1 | $E$ | An | 57.767 | 112.15 | 64b |
| An0.1–1 | $r_0$ | An | 1.17519 | 0.024815 | 64c |
| $RT \ln D$ REE regressions from An, linked to MgO (melt) by Eq. 3c, wet system, and $T$ (°C) by Eq.5a | | | | | |
| An<0.36288 | $\ln D_0$ | An | −3.3574 | −0.41784 | 65a |
| An0.36288–0.71581 | $\ln D_0$ | An | −1.3552 | 1.1444 | 65b |
| An0.71581–0.81764 | $\ln D_0$ | An | −0.1278 | −2.0230 | 65c |
| An>0.81764 | $\ln D_0$ | An | −0.5345 | −1.6905 | 65d |
| An<0.63045 | $E$ | An | 163.60 | 24.494 | 65a |
| An>0.63045 | $E$ | An | 57.767 | 112.149 | 65b |
| | $r_0$ | | | | Use Eq. 64c |
| $RT \ln D$ REE regressions from melt $SiO_2$, linked to $T$ (°C) by Eq.5b | | | | | |
| $SiO_2$40–45.81 | $\ln D_0$ | $SiO_2$ | −4.2516 | 0.03229 | 66a |
| $SiO_2$45.81–66.54 | $\ln D_0$ | $SiO_2$ | −5.1220 | 0.05130 | 66b |
| $SiO_2$66.54–78 | $\ln D_0$ | $SiO_2$ | −7.0283 | 0.07992 | 66c |
| $SiO_2$40–78 | $E$ | $SiO_2$ | −285.0 | −2.5 | 66d |
| $SiO_2$40–78 | $r_0$ | $SiO_2$ | 1.2221 | −0.000526 | 66e |
| $RT \ln D$ REE regressions for ferrar dolerite evolution, PELE Model, multiple regression using plagioclase An-conten and melt $SiO_2$ | | | | | |
| An0.786–0.692 | $\ln D_0$ | An | −1.1147 | −1.8677 | 67a |
| An0.786–0.692 | $E$ | An | 39.023 | 102.49 | 67b |
| | $r_0$ | | | | Use Eq. 64c |
| $RT \ln D$ REE regressions for high-Al arc basalt, PELE model, multiple regression using plagioclase An-conten and melt $SiO_2$ | | | | | |
| An0.88–0.80 | $\ln D_0$ | An | −3.31 | 0.46581 | 68a |
| An0.88–0.80 | $E$ | An | −169.53 | 351.95 | 68d |
| | $r_0$ | | | | use Eq. 64c |
| $RT \ln D$ REE regressions for MORB, multiple regression using plagioclase An-conten and melt $SiO_2$ | | | | | |
| An0.831–0.659 | $\ln D_0$ | An | −2.0363 | −0.82105 | 69a |
| An0.831–0.659 | $E$ | An | 104.64 | 23.3096 | 69b |
| | $r_0$ | | | | Use Eq. 64c |

dro's number; $R$ is the gas constant (0.008314), and $T$ is temperature (Kelvin). Values of $D_0$, $E$ and $r_0$ are commonly determined by fitting model curves to the experimental data (Fig. 14, see also Wood and Blundy, 1997). To this end, values of $r_0$, $E$ and $D_0$ were varied by trial and error to achieve a visual close fit to the $D$ REE regressions at a given value of plagioclase An-content (e.g. Fig. 14a and b). In view of the extensive scatter of the REE partitioning data (e.g. Fig. 12), more elaborate curve fitting methods would not improve accuracy and were not applied. It has been suggested (Bindeman and Davis, 2000) that the size of the M-site into which REE partition increases slightly as the An content decreases, and the fits appeared better if $r_0$ changed in this sense from 1.12 Å at $An_{100}$ to 1.178 Å at $An_{11}$. Values of $E$, and $\ln D_0$ derived in this manner were plotted against An and fit with simple functions after some trial and error optimisation (e.g. Fig. 15, Table 5). These regression constants (Table 5, Eqs. 64, cf. Fig. 12) allow values of $D_0$ and $E$ to be calculated for any input value of An; allowing a complete $D$ REE-Y profile to be calculated with Eq. (B).

A similar procedure was applied to the $RT \ln D$ REE regressions against plagioclase An-content for wet systems (Eqs. 65, Table 5) and against melt $SiO_2$ (Eqs. 66, Table 5, Fig. 14d and e, cf. Fig. 13a). The regressions based on changes in melt MgO produced spiky patterns that precluded accurate fits.

In order to use the multiple regression results (Eqs. 41–53c), an equation linking the pertinent input variables (e.g. An-content, and melt MgO and $SiO_2 \pm$ melt $H_2O$ content, $\pm$ pressure and $\pm \log f_{O_2}$ must be defined for the liquid line of descent being investigated. Given this information, the equations of Table 4 allow a series of $D$ REE-Y profiles to be defined, and fit as discussed above (e.g. Fig. 14c and f), to generate values of $r_0$, $D_0$ and $E$. Three suites were modeled (50–75% fractional crystallization) using PELE (Boudreau, 1999) to encompass variations of $D$ values for representative natural suites. The Ferrar Dolerite/Kirkpatrick Basalts of Antarctica illustrate a siliceous tholeiitic flood basalt trend. The fractionation model was based on sample 82-15-1 of Elliot et al. (1995), which is the most magnesian (7.542% MgO) non-porphyritic sample analyzed, with a calculated liquidus temperature of 1185 °C. An $f_{O2}$ at the QFM buffer (quartz–fayalite–magnetite) was assumed. Layered Ferrar sills (e.g. Bédard et al., 2005) contain minor biotite and hornblende, and ferrogabbroic pegmatites, suggesting that the magmas contained minor amounts of water. An initial value of 0.2 wt% $H_2O$ was assumed. Analysis 1 from Table 7 in Natland (1989), a glass from the Indian Ocean (8.97% MgO), was used as a typical primitive MORB-like melt. This yields a dry liquidus T of 1209 °C. An $f_{O_2}$ of QFM was assumed. A Tongan high-Al basalt (Table 2 in Myers and Johnson, 1996) was chosen to illustrate variations in an arc basalt. Here, a higher initial water content (2 wt%) and $f_{O_2}$ (QFM + 2) were used. Values for temperature, $f_{O_2}$, melt composition and feldspar An-content produced by PELE for these three compositions were recorded and used to calculate the $D$ values using (Eqs. 41c–53c Table 4). These were then fit with the Brice equation (e.g. Figs. 14c and f) to derive values of $E$ and $D_0$ (Eqs. 67–69, Table 5, Fig. 15). The value of $r_0$ was assumed to vary as in the generalized An regression (Eq. 64c). Values of $D$ calculated for the Ferrar suite are shown in many figures as a heavy black line (F: Figs. 3, 5, 7–10, 12, 13, 15) and typically plot in the main data cluster very close to the LSM trend for An or $SiO_2$.

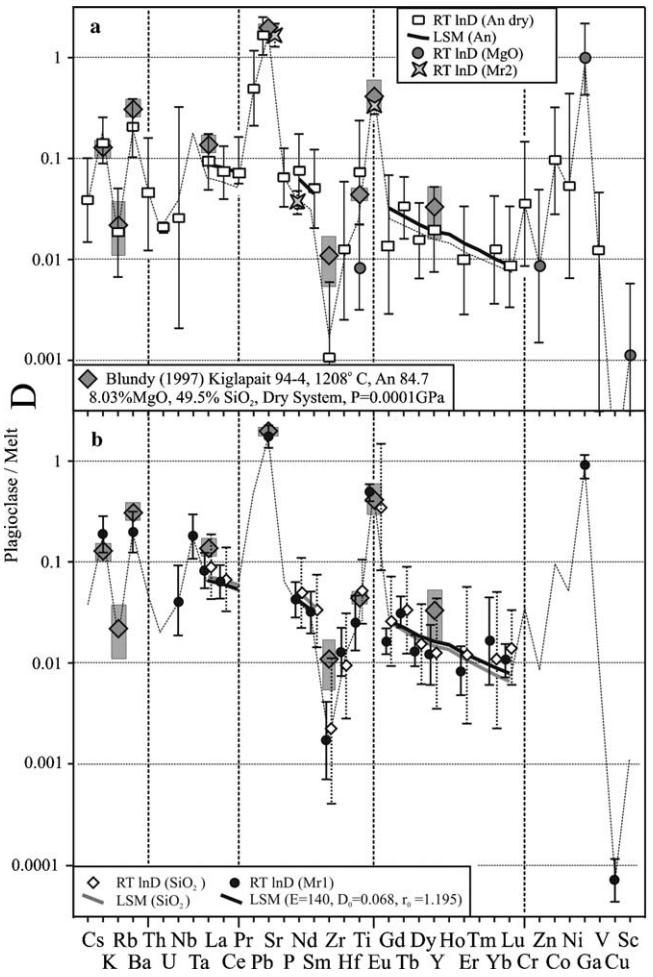


Fig. 16. Comparison of $^{plagioclase/melt}D$ profiles calculated from the different regression constants given in Tables 2–5, with $D$ results for experiment 94-4 from Blundy (1997). The grey boxes associated with the diamonds (i.e. the experimental data) show one sigma error limits; as do the error bars on the calculated values of $D$. The values for Mr1 are the preferred multiple regression results. Those labelled Mr2 are alternative formulations corresponding to Eqs. 19g, 44d and 46d. Lattice strain models (LSM) for An and $SiO_2$ use Eqs. 64 and 66 (respectively), while the LSM derived from the Mr1 regressions use values of $E$, $D_0$ and $r_0$ of 140, 0.068 and 1.195, respectively. The dashed line is the same for both a and b, and links the preferred $D$ values corresponding to Eqs. 16 (Cs), 15h (K), 17 (Rb), 18b (Ba), 37 (Th), 38a (U), 32b (Nb), 33 (Ta), LSM-Mr1 Eqs. 41c–42c (La–Ce), 20 (Pb), 19f (Sr), 39 (P), LSM-Mr1 Eqs. 44c-45c (Nd-Sm), 35 (Zr), 40c (Hf), 6 (Ti), 46c (Eu), LSM-Mr1 Eqs. 47c–53c (Gd–Lu), 23 (Cr), 31 (Zn), 29 (Co), 24 (Ni), 25b (Ga), 27 (V), 30 (Cu), and 28 (Sc).

## 4. Comparisons with partitioning data for individual experiments/samples

Values of *D* REE-Y calculated using the LSM parameterization (Table 5) are combined with *D* values calculated from the regressions of Tables 2–4, to produce multi-element *D* plots for different values of plagioclase An, melt MgO, melt $SiO_2$, melt $H_2O$, $f_{O_2}$, pressure and temperature (Fig. 16). The 1-σ error bars of the model profiles are attached to the best available regressions (see caption for Fig. 16). Note the generally small differences between results using the different regressions, and the fact that most of the experimental partitioning data are fit within error by the parameterization. Note also that the LSM fits to An, $SiO_2$ and Mr1 (multiple regression 1, see caption to Fig. 16) all yield very similar results.

Fig. 17 compares the model D profile to a series of individual experiments or observations, as a further test of the method. Each model was calculated using the MgO, $SiO_2$, An-content, pressure, temperature, $f_{O_2}$ and water content appropriate to each experiment or study. Overall, the experimental and natural data are very similar to the parameterization results (Fig. 17), suggesting that the methodology advocated in this paper has some merit. Note the prominent positive *D* Pb, Sr, Eu and Ga anomalies in the models and data. Because of the interrelations of the parameters feeding into the multiple regression equations for *D* Nb and *D* Ta, large negative *D* Nb–Ta anomalies are generated for intermediate systems. More experimental data for these elements are needed to verify if this is a real effect. The positive *D* Eu peak of the granite (Fig. 17d) is not reproduced by the parameterization, suggesting that the granite crystallized at values of $f_{O_2}$ different from that assumed. Values for *D* Zn, Ni, Ga and Co are high, with Ni and Ga becoming compatible elements in very evolved melts (Fig. 17d).

To give some feeling for the constraints gained by this parameterization, Fig. 18 shows the results of trace element inversion models (Bédard, 1994) that calculate the trace element contents of melts in equilibrium with three Bushveld anorthosites from the Merensky Reef, as compared to two putative parental melts (B1 and B2). Values of *D* were calculated for different assumed melt $SiO_2$ contents (Fig. 18b), but yield similar results except for Ta. Low assumed trapped melt fractions yield reasonable HREE matches with B2, while higher assumed trapped melt fractions better match the HREE of the more

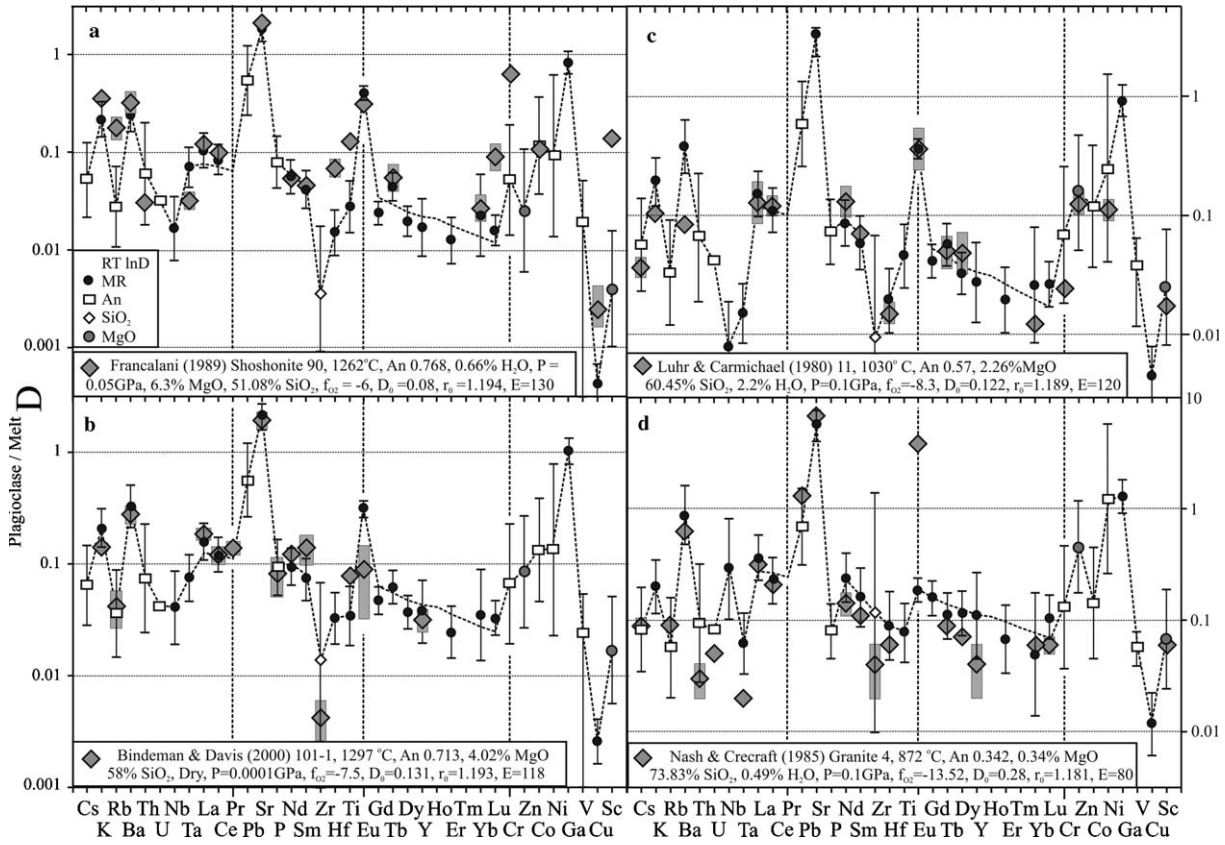


Fig. 17. Comparison of $^{plagioclase/melt}D$ profiles calculated from the different regression constants given in Tables 2–5, with the same equations as in the caption of Fig. 16. Model results are generally consistent with the data, with a few exceptions. Where no error bars are shown it is because they are smaller than the symbol size. (a) Francalanci (1989) model calculated assuming $P = 0.1$ GPa, temperatures assume a wet system (Eq. 3c), and $f_{O_2}$ was assumed to correspond to values of the quartz–fayalite–magnetite (QFM) buffer + 2. (b) The $f_{O_2}$ conditions in the experiments in Bindeman and Davis (2000) are not given, and were assumed to be at QFM. (c) The water content was assumed to be 2.2%, similar to other rocks in this study. (d) $f_{O_2}$ was assumed to be at QFM, with $P = 0.1$ GPa.

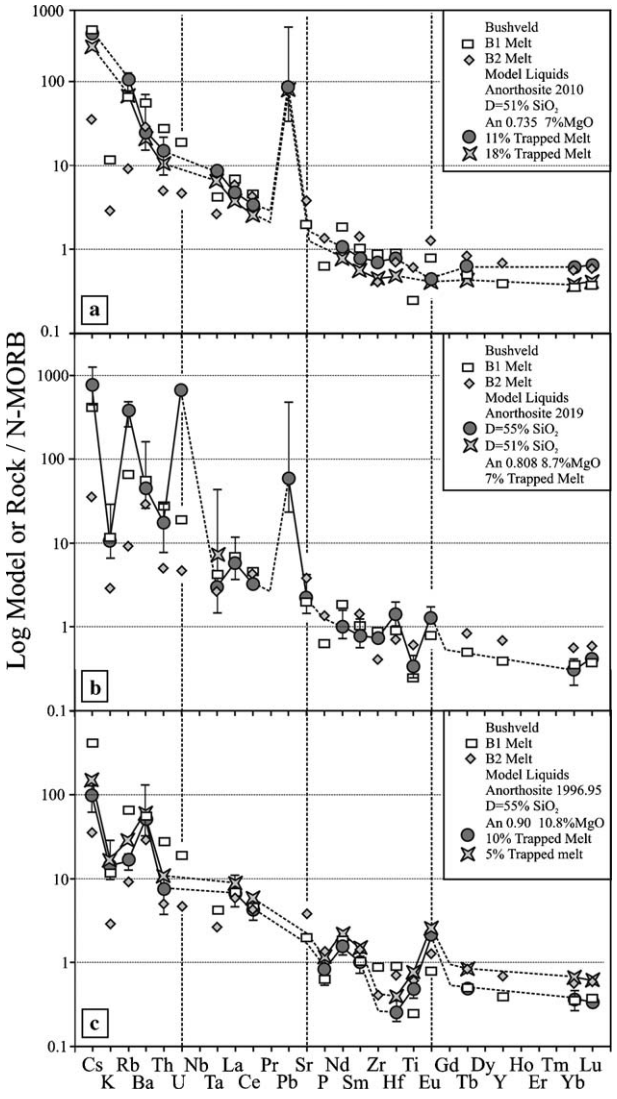


Fig. 18. N-MORB normalized (Sun and McDonough, 1989) extended trace element plots showing model melts calculated from three Bushveld anorthosites (data from Maier and Barnes, 1998; and W. Maier personal communication 2004) with the equilibrium distribution method of Bédard (1994) using the preferred $D$ values as per the caption of Fig. 17; compared to putative parental melts B1 and B2 (Harmer and Sharpe, 1985; W. Maier personal communication 2004). Values of $SiO_2$ in the melt were assumed to be either similar to those of melt B1 (55%) or B2 (51%); An-contents were calculated from a CIPW norm; MgO contents were calculated from Eq. 3a; and temperatures were estimated using Eq. 5a. Values of $f_{O_2}$ similar to those of Ferrar dolerite melts (QFM) were assumed. Model liquids calculated for these differing $SiO_2$ contents are directly compared in (b), and yield very similar results, except for Ta. $D$ REE are calculated from the regressions of $RT \ln D$ against An (Table 5, Eqs. 65, but with errors corresponding to Eqs. 67). Values of the trapped melt content are varied in (a and c), to force HREE fits with B1 and B2.

depleted siliceous B1 melt. The model melts have LILE contents that are more similar to B1 than B2, suggesting that B1 may be a better candidate for the melt responsible for Merensky Reef anorthosites. Trapped melt fractions between 7% and 18% imply a relatively low residual porosity for these rocks. Anorthosites 2019 and 1996.95 yield model melts with positive Eu anomalies, while 2019 shows a positive Sr anomaly, suggesting that the melts may have been supersaturated in plagioclase due to prior feldspar assimilation.

## 5. Conclusions

With a few exceptions, values of ${}^{\text{plagioclase/melt}}D$ increase as the anorthite-content of plagioclase decreases, as melt MgO decreases, and as melt $SiO_2$ increases. Values of ${}^{\text{plagioclase/melt}}D_{\text{Ti}}$ increase markedly as the melt $H_2O$ content increases, and as pressure drops, and the same may be true for ${}^{\text{plagioclase/melt}}D_{\text{REE}}$. Values of ${}^{\text{plagioclase/melt}}D_{\text{K}}$ and ${}^{\text{plagioclase/melt}}D_{\text{Sr}}$ are sensitive to pressure. Variations of $D_0$ (the strain compensated partition coefficient), $r_0$ (the size of the REE-hosting site), and $E$ (Young's modulus) were parameterized against variations of melt MgO, $SiO_2$, and the An-content of plagioclase, allowing ${}^{\text{plagioclase/melt}}D_{\text{REE-Y}}$ to be calculated from combinations of these input parameters. These parameterizations yield results comparable to experimental or natural partitioning data, and provide improved solutions to trace element models applied to plagioclase-bearing systems.

## Acknowledgments

Datasets were provided by: Gaëlle Prouteau, Jasper Berndt, Jurgen Koepke, A. Patino-Douce, M. Pertermann, François Holtz, A. Garcia-Casco, Bruno Scaillet, Gerhardt Wörner, Peter Michael, Carrie Brugger, Dana Johnston, S. Couch, Wolfgang Maier and Tom Sisson; and their generosity is gratefully acknowledged. Jon Blundy helped with the lattice strain calculations. Several anonymous reviews and comments by Louise Corriveau and Gerhard Wörner helped refine the paper. This is Geological Survey of Canada contribution # 20060048.

*Associate editor:* Clive R. Neal

## References

Albarède, F., Bottinga, Y., 1972. Kinetic disequilibrium in trace element partitioning between phenocrysts and host lava. *Geochim. Cosmochim. Acta* **36**, 141–156.

Arth, J.G., Barker, F., 1976. Rare-earth partitioning between hornblende and dacite liquid and implications for the origin of trondhjemitic–tonalitic magmas. *Geology* **4**, 534–536.

Bacon, C.R., Druitt, T.H., 1988. Compositional evolution of the zoned calcalkaline magma chamber of Mount Mazama, Crater Lake, Oregon. *Contrib. Mineral. Petrol.* **98**, 224–256.

Baker, D.R., Eggler, D.H., 1987. Compositions of anhydrous melts coexisting with plagioclase, augite and olivine or low-Ca pyroxene from 1 atm to 8 kbar: aapplication to the Aleutian volcanic center of Atka. *Am. Mineral.* **72**, 12–28.

Bartels, K.S., Kinzler, R.J., Grove, T.L., 1991. High pressure phase relations of primitive high-alumina basalts from Medicine Lake Volcano, northern California. *Contrib. Mineral. Petrol.* **108**, 253–270.

Beard, J.S., Abitz, R.J., Lofgren, G.E., 1993. Experimental melting of crustal xenoliths from Kilbourne Hole, New Mexico and implications for the contamination and genesis of magmas. *Contrib. Mineral. Petrol.* **115**, 88–102.

Beattie, P., Ford, C., Russell, D., 1991. Partition coefficients for olivine-melt and orthopyroxene-melt systems. *Contrib. Mineral. Petrol.* **109**, 212–224.

Beckett, J.R., Grossman, L., 1988. The origin of type C inclusions from carbonaceous chondrites. *Earth Planet. Sci. Lett.* **89**, 1–14.

Bédard, J.H., 1994. A procedure for calculating the equilibrium distribution of trace elements among the minerals of cumulate rocks, and the concentration of trace elements in the coexisting liquids. *Chem. Geol.* **118**, 143–153.

Bédard, J.H., 2001. Parental magmas of the Nain Plutonic Suite anorthosites and mafic cumulates: a trace element modelling approach. *Contrib. Mineral. Petrol.* **141**, 747–771.

Bédard, J.H., Fleming, T., Hersum, T., Marsh, B., Mathez, E., Mukasa, S.B., Naslund, H.R., Simon, A. 2005. *Evidence for Channelized Transfer of Residual Melts and Fluids in the Basement Sill, Ferrar Province, Antarctica.* EOS Trans. Am. Geophys. Union, San Francisco, V14C-05.

Berndt, J. 2002. *Differentiation of MOR Basalt at 200 MPa: Experimental Techniques and Influence of $H_2O$ and $f_{O_2}$ on Phase Relations and Liquid Line of Descent.* PhD Dissertaition, Universität Hannover, Germany, p. 118.

Berndt, J., Holtz, F., Koepke, J., 2001. Experimental constraints on storage conditions in the chemically zoned phonolitic magma chamber of the Laacher See volcano. *Contrib. Mineral. Petrol.* **140**, 469–486.

Bindeman, I.N., Davis, A.M., 2000. Trace element partitioning between plagioclase and melt: investigation of dopant influence on partition behavior. *Geochim. Cosmochim. Acta* **64**, 2863–2878.

Bindeman, I.N., Davis, A.M., Drake, M.J., 1998. Ion microprobe study of plagioclase-basalt partition experiments at natural concentration levels of trace elements. *Geochim. Cosmochim. Acta* **62**, 1175–1193.

Blatter, D.L., Carmichael, I.S.E., 2001. Hydrous phase equilibria of a Mexican high-silica andesite: a candidate for a mantle origin? *Geochim. Cosmochim. Acta* **65**, 4043–4065.

Blundy, J., 1997. Experimental study of a Kiglapait marginal rock and implications for trace element partitioning in layered intrusions. *Chem. Geol.* **141**, 73–92.

Blundy, J.D., Robinson, J.A.C., Wood, B.J., 1998. Heavy REE are compatible in clinopyroxene on the spinel lherzolite solidus. *Earth Planet. Sci. Lett.* **160**, 493–504.

Blundy, J.D., Wood, B.J., 1991. Crystal-chemical controls on the partitioning of Sr and Ba between plagioclase feldspar, silicate melts, and hydrothermal solutions. *Geochim. Cosmochim. Acta* **55**, 193–209.

Blundy, J.D., Wood, B.J., 1994. Prediction of crystal-melt partition coefficients from elastic moduli. *Nature* **372**, 452–454.

Blundy, J.D., Wood, B.J., 2003. Partitioning of trace elements between crystals and melts. *Earth Planet. Sci. Lett.* **210**, 383–397.

Blundy, J.D., Wood, B.J., Davies, A., 1996. Thermodynamics of rare earth element partitioning between clinopyroxene and melt in the system $CaO–MgO–Al_2O_3–SiO_2$. *Geochim. Cosmochim. Acta* **60**, 359–364.

Boudreau, A.E., 1999. PELE—a version of the MELTS software program for the PC platform. *Comp. Geosci.* **25**, 201–203.

Bowen, N.L., 1928. *The Evolution of the Igneous Rocks*. Princeton University Press, Princeton, NJ, p. 334.

Brice, J.C., 1975. Some thermodynamic aspects of the growth of strained crystals. *J. Crystal Growth* **28**, 249–253.

Brugger, C.R., Johnston, A.D., Cashman, K.V., 2003. Phase relations in silicic systems at one-atmosphere pressure. *Contrib. Mineral. Petrol.* **146**, 356–369.

Capobianco, C.J., Drake, M.J., Rogers, P.S.Z., 1991. Crystal/melt partitioning of Ru, Rh and Pd for silicate and oxide phases. *Lunar Planet. Sci.* **22**, 179–180.

Carroll, M.R., Wyllie, P.J., 1989. Experimental phase relations in the system tonalite–peridotite–$H_2O$ at 15: implications for assimilation and differentiation processes near the crust–mantle boundary. *J. Petrol.* **30**, 1351–1382.

Couch, S., Harford, C.L., Sparks, R.S.J., Carroll, M.R., 2003. Experimental constraints on the conditions of formation of highly calcic plagioclase microlites at the Soufrière Hills Volcano, Montserrat. *J. Petrol.* **44**, 1455–1475.

Costa, F., Scaillet, B., Pichavant, M., 2004. Petrological and experimental constraints on the pre-eruption conditions of Holocene dacite from Volcan San Pedro (36°S, Chilean Andes) and the importance of sulphur in silicic subduction-related magmas. *J. Petrol.* **45**, 855–881.

Dodge, F.C.W., Millard, H.T., Elsheimer, H.N., 1982. *Compositional Variations and Abundances of Selected Elements in Granitoid Rocks and Constituent Minerals, Central Sierra Nevada batholith, California*. US geol. Surv. Prof. Paper 1248, p. 24.

Dostal, J., Capedri, S., 1975. Partition coefficients of uranium for some rock-forming minerals. *Chem. Geol.* **15**, 285–294.

Dostal, J., Dupuy, C., Carron, J.P., LeGuen de Kerneizon, M., Maury, R.C., 1983. Partition coefficients of trace elements: application to volcanic rocks of St.Vincent, West Indies. *Geochim. Cosmochim. Acta* **47**, 525–533.

Douce, A.E.P., 2005. Vapor-absent melting of tonalite at 15–32 kbar. *J. Petrol.* **46**, 275–290.

Douce, A.E.P., Beard, J.S., 1995. Dehydration-melting of biotite gneiss and quartz amphibolite from 3 to 15 kbar. *J. Petrol.* **36**, 707–738.

Douce, A.E.P., Beard, J.S., 1996. Effects of P, $f_{O_2}$ and Mg/Fe ratio on dehydration melting of model metagreywackes. *J. Petrol.* **37**, 999–1024.

Douce, A.E.P., Harris, N., 1998. Experimental constraints on Himalayan anatexis. *J. Petrol.* **39**, 689–710.

Drake, M.J., Weill, D., 1975. Partition of Sr, Ba, Ca, Y, $Eu^{2+}$, $Eu^{3+}$, and other REE between plagioclase feldspar and magmatic liquid: an experimental study. *Geochim. Cosmochim. Acta* **39**, 689–712.

Dudas, M.J., Schmitt, R.A., Harward, M.E., 1971. Trace element partitioning between volcanic plagioclase and dacitic pyroclastic matrix. *Earth Planet. Sci. Lett.* **11**, 440–446.

Duncan, R.A., Green, D.H., 1987. The genesis of refractory melts in the formation of oceanic crust. *Contrib. Mineral. Petrol.* **96**, 326–342.

Dunn, T., Sen, C., 1994. Mineral/matrix partition coefficients for orthopyroxene, plagioclase, and olivine in basaltic to andesitic systems: a combined analytical and experimental study. *Geochim. Cosmochim. Acta* **58**, 717–733.

Elliot, D.H., Fleming, T.H., Haban, M.A., Siders, M.A., 1995. Petrology and mineralogy of the Kirkpatrick Basalt and Ferrar dolerite, Mesa Range region, north Victoria Land, Antarctica. In: Elliott, G.L., Blaisdell G.L. (eds), *Contributions to Antarctic Research IV* Am. Geophys. Union Antarctic Research Series, Washington, DC, pp. 103–141.

Ewart, A., Griffin, W.L., 1994. Application of proton-microprobe data to trace-element partitioning in volcanic rocks. *Chem. Geol.* **117**, 251–284.

Falloon, T.J., Green, D.H., Jacques, A.L., Hawkins, J.W., 1999. Refractory magmas in back-arc basin settings—experimental constraints on the petrogenesis of a Lau Basin example. *J. Petrol.* **40**, 255–277.

Francalanci, L., 1989. Trace element partitioning coefficients for minerals in shoshonitic and calc-alkaline rocks from Stromboli Island (Aeolian Arc). *Neues Jahrbuch Miner. Abh.* **160**, 229–247.

Fram, M.S., Longhi, J., 1992. Phase equilibria of dikes associated with Proterozoic anorthosite complexes. *Am. Mineral.* **77**, 605–616.

Freise, M., Holtz, F., Koepke, J., Scoates, J., Leyrit, H., 2003. Experimental constraints on the storage conditions of phonolites from the Kerguelen Archipelago. *Contrib. Mineral. Petrol.* **145**, 659–672.

Fujimaki, H., Tatsumoto, M., Aoki, K. 1984. Partition coefficients of Hf, Zr and REE between phenocrysts and groundmass. *Proc. 14th Lunar Planet. Sci. Conf. Part 2, J. Geophys. Res.* vol. 89, Suppl. B662–672.

Gaetani, G.A., 2004. The influence of melt structure on trace element partitioning near the peridotite solidus. *Contrib. Mineral. Petrol.* **147**, 511–527.

García-Casco, A., Haissen, F., Castro, A., El-Hmidi, H., Torres-Roldán, R.L., Millán, G., 2003. Synthesis of staurolite in melting experiments of a natural metapelite: consequences for the phase relations in low-temperature pelitic migmatites. *J. Petrol.* **44**, 1727–1757.

Gass, I.G., Lippard, S.J., Shelton, A.W., 1984. *Ophiolites and Oceanic Lithosphere: Geol. Soc. London Spec. Publ.* 13, p. 413.

Gerke, T.L., Kilinc, A.I., Sack, R.O., 2005. Ti-content of high-Ca pyroxenes as a petrogenetic indicator: an experimental study of mafic alkaline rocks from the Mt. Erebus volcanic region, Antarctica. *Contrib. Mineral. Petrol.* **148**, 735–745.

Green, T.H., Pearson, N.J., 1985. Rare earth element partitioning between clinopyroxene and silicate liquid at moderate to high pressure. *Contrib. Mineral. Petrol.* **91**, 24–36.

Gromet, L.P., Silver, L.T., 1983. Rare-earth element distributions among minerals in a granodiorite and their petrogenetic implications. *Geochim. Cosmochim. Acta* **47**, 925–939.

Grove, T.L., Elkins-Tanton, L.T., Parman, S.W., Chatterjee, N., Müntener, O., Gaetani, G.A., 2003. Fractional crystallization and mantle-melting controls on calc-alkaline differentiation trends. *Contrib. Mineral. Petrol.* **145**, 515–533.

Grove, T.L., Gerlach, D.C., Sando, T.W., 1982. Origin of calc-alkaline series lavas at Medicine Lake volcano by fractionation, assimilation and mixing. *Contrib. Mineral. Petrol.* **80**, 160–182.

Grove, T.L., Juster, T.C., 1989. Experimental investigations of low-Ca pyroxene stability and olivine–pyroxene–liquid equilibria at 1-atm in natural basaltic and andesitic liquids. *Contrib. Mineral. Petrol.* **103**, 287–305.

Harmer, R.E., Sharpe, M.R., 1985. Field relations and strontium isotope systematics of the eastern Bushveld complex. 80, 813–837.

Holtz, F., Sato, H., Lewis, J., Behrens, H., Nakada, S., 2005. Experimental petrology of the 1991–1995 Unzen dacite, Japan. Part I: phase relations, phase composition and pre-eruptive conditions. *J. Petrol.* **46**, 319–337.

Housh, T.B., Luhr, J.F., 1991. Plagioclase-melt equilibria in hydrous systems. *Am. Mineral.* **76**, 477–492.

Johnston, A.D., 1986. Anhydrous *P–T* phase relations of near-primary high-alumina basalt from the South Sandwich Islands. *Contrib. Mineral. Petrol.* **92**, 368–382.

Kinzler, R.J., Grove, T.L., 1992. Primary magmas of mid-ocean ridge basalts .1. Experiments and methods. *J. Geophys. Res.* **97**, 6885–6906.

Koepke, J., Berndt, J., Bussy, F., 2003. An experimental study on the shallow-level migmatization of ferrogabbros from the Fuerteventura Basal Complex, Canary Islands. *Lithos* **69**, 105–125.

Langmuir, C.H., 1989. Geochemical consequences of in situ crystallization. *Nature* **340**, 199–205.

Larsen, J.F., 2005. Experimental study of plagioclase rim growth around anorthite seed crystals in rhyodacitic melt. *Am. Mineral.* **90**, 417–427.

Longhi, J., Van der Auwera, J., Fram, M.S., Duchesne, J.C., 1999. Some phase equilibrium constraints on the origin of Proterozoic (Massif) anorthosites and related rocks. *J. Petrol.* **40**, 339–362.

López, S., Castro, A., 2001. Determination of the fluid-absent solidus and supersolidus phase relationships of MORB-derived amphibolites in the range 4-14 kbar. *Am. Mineral.* **86**, 1396–1403.

López, S., Castro, A., Garcia-Casco, A., 2005. Production of granodiorite melt by interaction between hydrous mafic magma and tonalitic crust. Experimental constraints and implications for the generation of Archaean TTG complexes. *Lithos* **79**, 229–250.

Loucks, R.R., 1996. Restoration of the elemental and stable-isotopic compositions of diffusionally altered minerals in slowly cooled rocks. *Contrib. Mineral. Petrol.* **124**, 346–358.

Luhr, J.F., Carmichael, I.S.E., 1980. The Colima volcanic complex, Mexico, I. Post-caldera andesites from Volcan Colima. *Contrib. Mineral. Petrol.* **71**, 343–372.

Lutz, T.M., 1991. Trace element and isotopic zoning in minerals—models of compositional fractionation by mineral separation procedures. *Lithos* **27**, 1–11.

Maier, W.D., Barnes, S.J., 1998. Concentrations of rare earth elements in silicate rocks of the Lower, Critical and Main Zones of the Bushveld Complex. *Chem. Geol.* **150**, 85–103.

Malvin, D.J., Drake, M.J., 1987. Experimental determination of crystal/melt partitioning of Ga and Ge in the system forsterite–anorthite–diopside. *Geochim. Cosmochim. Acta* **51**, 2117–2128.

Markl, G., Frost, B.R., 1999. The origin of anorthosites and related rocks from the Lofoten Islands, northern Norway: II. Calculation of parental liquid compositions for anorthosites. *J. Petrol.* **40**, 61–77.

Martel, C., Pichavant, M., Holtz, F., Scaillet, B., Bourdier, J.L., Traineau, H., 1999. Effects of $f_{O_2}$ and $H_2O$ on andesite phase relations between 2 and 4 kbar. *J. Geophys. Res.* **104**, 29453–29470.

Métrich, N., Rutherford, M.J., 1998. Low pressure crystallization paths of $H_2O$-saturated basaltic-hawaiitic melts from Mt Etna: implications for open-system degassing of basaltic volcanoes. *Geochim. Cosmochim. Acta* **62**, 1195–1205.

McDonough, W.F., Stosch, H.G., Ware, N.G., 1992. Distribution of titanium and the rare earth elements between peridotitic minerals. *Contrib. Mineral. Petrol.* **110**, 321–328.

McKay, G.A., Weill, D.F., 1977. KREEP petrogenesis revisited. *Proc. Eighth Lunar Sci. Conf.*, 2339–2355.

McKay, G.A., Weill, D.F., 1976. The petrogenesis of KREEP. *Proc. Seventh Lunar Sci. Conf.*, 2427–2447.

Médard, E., Schmidt, M.W., Schiano, P., 2004. Liquidus surfaces of ultracalcic primitive melts: formation conditions and sources. *Contrib. Mineral. Petrol.* **148**, 201–215.

Michael, P.J., 1983. Chemical differentiation of the Bishop Tuff and other high-silica magmas through crystallization processes. *Geology* **11**, 31–34.

Michael, P.J., 1988. Partition coefficients for rare earth elements in mafic minerals of high silica rhyolites: the importance of accessory mineral inclusions. *Geochim. Cosmochim. Acta* **52**, 275–282.

Montel, J.M., Vielzeuf, D., 1997. Partial melting of metagreywackes. 2. Compositions of minerals and melts. *Contrib. Mineral. Petrol.* **128**, 176–196.

Moore, G.M., Carmichael, I.S.E., 1998. The hydrous phase equilibria (to 3 kbar) of an andesite and basaltic andesite from western Mexico: constraints on water content and conditions of phenocryst growth. *Contrib. Mineral. Petrol.* **130**, 304–319.

Müntener, O., Kelemen, P.B., Grove, T.L., 2001. The role of $H_2O$ during crystallization of primitive arc magmas under uppermost mantle conditions and genesis of igneous pyroxenites: an experimental study. *Contrib. Mineral. Petrol.* **141**, 643–658.

Myers, J.D. , Johnson, A.D., 1996. Phase equilibria constraints on models of subduction zone magmatism. In: Bebout, G.E., Scholl, D.W., Kirby, S.H., Platt, J.P., (eds.), *Subduction, Top to Bottom* American Geophys. Union Monograph vol. 96, Washington, DC, pp. 229–249.

Mysen, B.O., Virgo, D., 1980. Trace element partitioning and melt structure: an experimental study at 1 atm pressure. *Geochim. Cosmochim. Acta* **44**, 1917–1930.

Nagasawa, H., Schnetzler, C.C., 1971. Partitioning of rare earth, alkali and alkaline earth elements between phenocrysts and acidic igneous magma. *Geochim. Cosmochim. Acta* **35**, 953–968.

Nair, R., Chacko, T., 2002. Fluid-absent melting of high-grade semipelites: *P–T* constraints on orthopyroxene formation and implications for granulite genesis. *J. Petrol.* **43**, 2121–2141.

Nash, W.P., Crecraft, H.R., 1985. Partition coefficients for trace elements in silicic magmas. *Geochim. Cosmochim. Acta* **49**, 2309–2322.

Natland, J.H., 1989. Partial melting of lithologically heterogeneous mantle: inferences from crystallization histories of magnesian abyssal tholeiites from the Siqueiros Fracture Zone. In: Saunders, A.D., Norry, M.J. (Eds.), *Magmatism in the Ocean Basins*, *Geol. Soc. London Spec. Publ.*, 42. Blackwell Publ., pp. 41–70.

Nekvasil, H., Dondolini, A., Horn, J., Filiberto, J., Long, H., Lindsley, D.H., 2004. The origin and evolution of silica-saturated alkalic suites: an experimental study. *J. Petrol.* **45**, 693–721.

Nielsen, R.L., 1985. A method for the elimination of the compositional dependence of trace element distribution coefficients. *Geochim. Cosmochim. Acta* **49**, 1775–1779.

O'Hara, M.J., 1995. Trace element geochemical effects of integrated melt extraction and 'shaped' melting regimes. *J. Petrol.* **36**, 1111–1132.

Panjasawatwong, Y., Danyushevsky, L.V., Crawford, A.J., Harris, K.L., 1995. An experimental study of the effects of melt composition on plagioclase—melt equilibria at 5 and 10 kbar: implications for the

origin of magmatic high-An plagioclase. *Contrib. Mineral. Petrol.* **118**, 420–432.

Pertermann, M., Hirschmann, M.M., Hametner, K., Gunther, D., Schmidt, M.W., 2004. Experimental determination of trace element partitioning between garnet and silica-rich liquid during anhydrous partial melting of MORB-like eclogite. art. # Q05A01, *Geochem. Geophys. Geosyst.* vol. 5.

Perugini, D., Poli, G., Mazzuoli, R., 2003. Chaotic advection, fractals and diffusion during mixing of magmas: evidence from lava flows. *J. Volcanol. Geotherm. Res.* **124**, 255–279.

Phinney, W.C., Morrison, D.A., 1990. Partition coefficients for calcic plagioclase: implications for Archean anorthosites. *Geochim. Cosmochim. Acta* **54**, 1639–1654.

Prouteau, G., Scaillet, B., 2003. Experimental constraints on the origin of the 1991 Pinatubo dacite. *J. Petrol.* **44**, 2203–2241.

Ren, M.H., Parker, D.F., White, J.C., 2003. Partitioning of Sr, Ba, Rb, Y, and LREE between plagioclase and peraluminous silicic magma. *Am. Mineral.* **88**, 1091–1103.

Righter, K., Capobianco, C.J., Drake, M.J., 1995. Experimental constraints on the partitioning of Re between augite, olivine, melilite and silicate liquid at high oxygen fugacities (>NNO). *EOS Trans. AGU* **76**, F698.

Scaillet, B., Evans, B.W., 1999. The 15 June 1991 eruption of Mount Pinatubo. I. Phase equilibria and pre-eruption $P$–$T$–$f_{O_2}$–$f_{H_2O}$ conditions of the dacite magma. *J. Petrol.* **40**, 381–411.

Schnetzler, C.C., Philpotts, J.A., 1968. Partition coefficients of rare-earth elements and Barium between igneous matrix material and rock-forming mineral phenocrysts n I. *Geochim. Cosmochim. Acta* **32**, 929–938.

Schmidt, M.W., Thompson, A.B., 1996. Epidote in calc-alkaline magmas: an experimental study of stability, phase relationships, and the role of epidote in magmatic evolution. *Am. Mineral.* **81**, 462–474.

Shannon, R.D., 1976. Revised effective ionic raii and systematic studies of interatomic distances in halides and chalcogenides. *Acta Crystallogr.* **A32**, 751–767.

Shaw, D.M., 2000. Continuous (Dynamic) melting theory revisited. *Can. Mineral.* **38**, 1041–1063.

Shimizu, N., 1974. An experimental study of the partitioning of K, Rb, Cs, Sr, and Ba between clinopyroxene and liquid at high pressures. *Geochim. Cosmochim. Acta* **38**, 1789–1798.

Simon, S.B., Kuehner, S.M., Davis, A.M., Grossman, L., Johnson, M.L., Burnett, D.S., 1994. Experimental studies of trace element partitioning in Ca, Al-rich compositions: anorthite and perovskite. *Geochim. Cosmochim. Acta* **58**, 1507–1523.

Singh, J., Johannes, W., 1996. Dehydration melting of tonalites. 2. Composition of melts and solids. *Contrib. Mineral. Petrol.* **125**, 26–44.

Sisson, T.W., Ratajeski, K., Hankins, W.B., Glazner, A.F., 2005. Voluminous granitic magmas from common basaltic sources. *Contrib. Mineral. Petrol.* **148**, 635–661.

Skjerlie, K.P., Johnston, A.D., 1996. Vapour-absent melting from 10 to 20 kbar of crustal rocks that contain multiple hydrous phases: implications for anatexis in the deep to very deep continental crust and active continental margins. *J. Petrol.* **37**, 661–691.

Smith, J.V. Brown, W.L., 1988. *Feldspar Minerals*, vol I, Springer-Verlag.

Springer, W., Seck, H.A., 1997. Partial fusion of basic granulites at 5 to 15 kbar: implications for the origin of TTG magmas. *Contrib. Mineral. Petrol.* **127**, 30–45.

Spulber, S.D., Rutherford, M.J., 1983. The origin of rhyolite and plagiogranite in oceanic crust: an experimental study. *J. Petrol.* **24**, 1–25.

Sugawara, T., 2000. Empirical relationships between temperature, pressure, and MgO content in olivine and pyroxene saturated liquid. *J. Geophys. Res.* **105**, 8457–8472.

Sun, S.-S., McDonough, W.F., 1989. Chemical and isotopic systematics of oceanic basalts: implications for mantle compositions and processes. In: Saunders, A.D., Norry, M.J. (Eds.), *Magmatism in the Ocean Basins*, *Geol. Soc. Lond. Spec. Publ.*, 42. Blackwell Publ, pp. 313–345.

Takagi, D., Sato, H., Nakagawa, M., 2005. Experimental study of a low-alkali tholeiite at 1–5 kbar: optimal condition for the crystallization of high-An plagioclase in hydrous arc tholeiite. *Contrib. Mineral. Petrol.* **149**, 527–540.

Tepley, F.J., Davidson, J.P., Tilling, R.I., Arth, J.G., 2000. Magma mixing, recharge and eruption histories recorded in plagioclase phenocrysts from El Chichon Volcano, Mexico. *J. Petrol.* **41**, 1397–1411.

Thompson, R.N., Morrison, M.A., Dickin, A.P., Hendry, G.L., 1983. Continental flood basalts ... Arachnids rule OK? In: Hawkesworth, C.J., Norry, M.J. (Eds.), *Continental Basalts and Mantle Xenoliths*. Shiva Publishing Ltd, Cheshire, U.K., pp. 158–185.

Thy, P., 1995. Experimental constraints on the evolution of transitional and mildly alkalic basalts: Crystallization of spinel. *Lithos* **36**, 103–114.

Toplis, M.J., Carroll, M.R., 1995. An experimental study of the influence of oxygen fugacity on Fe–Ti oxide stability, phase relations, and mineral-melt equilibria in ferro-basaltic systems. *J. Petrol.* **36**, 1137–1170.

Toplis, M.J., Libourel, G., Carroll, M.R., 1994. The role of phosphorus in crystallisation processes of basalt: an experimental study. *Geochim. Cosmochim. Acta* **58**, 797–810.

Tormey, D.R., Grove, T.L., Bryan, W.B., 1987. Experimental petrology of normal MORB near the Kane Fracture Zone: 22°–25°N, mid-Atlantic ridge. *Contrib. Mineral. Petrol.* **82**, 121–139.

Treuil, M., Varet, J., 1973. Critères volcanologiques, pétrologiques et géochimiques de la genèse et de la différenciation des magmas basaltiques: exemple de l'Afar. *Bull. soc. géol. France* **7**, 506–540.

Tuff, J., Takahashi, E., Gibson, S.A., 2005. Experimental constraints on the role of garnet pyroxenite in the genesis of high-Fe mantle plume derived melts. *J. Petrol.* **46**, 2023–2058.

Van der Auwera, J., Longhi, J., Duchesne, J.C., 2000. The effect of pressure on $^{plag/melt}D_{Sr}$ and $^{opx/melt}D_{Cr}$ : implications for anorthosite petrogenesis. *Earth Planet. Sci. Lett.* **178**, 303–314.

Vernières, J., Joron, J.L., Treuil, M., Coulon, C., Dupuy, C., 1977. Coéfficient de partage de quelques éléments en trace entre plagioclase et verre dans les ignimbrites—implications pétrogénétiques. *Chem. Geol.* **19**, 309–325.

Villemant, B., Joron, J.L., Jaffrezic, H., Treuil, M., Maury, R.C., Brousse, R., 1980. Cristallisation fractionnée d'un magma basaltique alcalin: la série de la Chaîne des Puys (Massif Central, France). III: Géochimie. *Bull. Mineral.* **103**, 267–286.

Villiger, S., Ulmer, P., Müntener, O., Thompson, A.B., 2004. The liquid line of descent of anhydrous, mantle-derived, tholeiitic liquids by fractional and equilibrium crystallization—an experimental study at 1.0 GPa. *J. Petrol.* **45**, 2369–2388.

Wilke, M., Behrens, H., 1999. The dependence of the partitioning of iron and europium between plagioclase and hydrous tonalitic melt on oxygen fugacity. *Contrib. Mineral. Petrol.* **137**, 102–114.

Wood, B.J., Blundy, J.D., 1997. A predictive model for rare earth element partitioning between clinopyroxene and anhydrous silicate melt. *Contrib. Mineral. Petrol.* **129**, 166–181.

Wood, B.J., Blundy, J.D., 2002. The effect of $H_2O$ on crystal-melt partitioning of trace elements. *Geochim. Cosmochim. Acta* **66**, 3647–3656.

Wörner, G., Beusen, J.-M., Duchateau, N., Gijbels, R., Schmincke, H.-U., 1983. Trace element abundances and mineral/melt distribution coefficients in phonolites from the Laacher See Volcano (Germany). *Contrib. Mineral. Petrol.* **84**, 152–173.

Yang, H.J., Kinzler, R.J., Grove, T.L., 1996. Experiments and models of anhydrous, basaltic olivine–plagioclase–augite saturated melts from 0.001 to 10 kbar. *Contrib. Mineral. Petrol.* **124**, 1–18.